The Complexity of the Cetus Stream Unveiled from the Fusion of STREAMFINDER and StarGO

Zhen Yuan, Khyati Malhan, Federico Sestito, Rodrigo A. Ibata, Nicolas F. Martin, Jiang Chang, Ting S. Li, Elisabetta Caffau, Piercarlo Bonifacio, Michele Bellazzini, et al.

The Astrophysical Journal, 930:103 (16pp), 2022 May 10 https://doi.org/10.3847/1538-4357/ac616f

The Complexity of the Cetus Stream Unveiled from the Fusion of STREAMFINDER and StarGO

Zhen Yuan[1], Khyati Malhan[2], Federico Sestito[3], Rodrigo A. Ibata[1], Nicolas F. Martin[1,2], Jiang Chang[4], Ting S. Li[5], Elisabetta Caffau[6], Piercarlo Bonifacio[6], Michele Bellazzini[7], Yang Huang[8], Karina Voggel[1], Nicolas Longeard[9], Anke Arentsen[1], Amandine Doliva-Dolinsky[1], Julio Navarro[3], Benoit Famaey[1], Else Starkenburg[10], and David S. Aguado[11]

[1] Université de Strasbourg, CNRS, Observatoire Astronomique de Strasbourg, UMR 7550, F-67000 Strasbourg, France; zhen.yuan@astro.unistra.fr
[2] Max-Planck-Institut für Astronomie, Königstuhl 17, D-69117, Heidelberg, Germany
[3] Department of Physics and Astronomy, University of Victoria, Victoria, BC V8W 3P2, Canada
[4] Purple Mountain Observatory, CAS, No. 10 Yuanhua Road, Qixia District, Nanjing 210034, People's Republic of China
[5] Department of Astronomy and Astrophysics, University of Toronto, 50 Saint George Street, Toronto ON, M5S 3H4, Canada
[6] GEPI, Observatoire de Paris, Université PSL, CNRS, 5 Place Jules Janssen, F-92190 Meudon, France
[7] INAF–Osservatorio di Astrofisica e Scienza dello Spazio, via Gobetti 93/3, I-40129 Bologna, Italy
[8] South-Western Institute for Astronomy Research, Yunnan University, Kunming 650500, People's Republic of China
[9] Laboratoire d'astrophysique, École Polytechnique Fédérale de Lausanne (EPFL), Observatoire, 1290 Versoix, Switzerland
[10] Kapteyn Astronomical Institute, University of Groningen, Landleven 12, NL-9747 AD Groningen, The Netherlands
[11] Dipartimento di Fisica e Astrofisica, Univerisitá degli Studi di Firenze, via Giovanni Sansone 1, Sesto Fiorentino I-50019, Italy
Received 2021 December 1; revised 2022 March 14; accepted 2022 March 25; published 2022 May 9

Abstract

We combine the power of two stream-searching tools, `STREAMFINDER` and `StarGO` applied to the Gaia EDR3 data, to detect stellar debris belonging to the Cetus stream system that forms a complex, nearly polar structure around the Milky Way. In this work, we find the southern extensions of the northern Cetus stream as the Palca stream and a new southern stream, which overlap on the sky but have different distances. These two stream wraps extend over more than $\sim$100° on the sky ($-60° < \delta < +40°$). The current *N*-body model of the system reproduces both as two wraps in the trailing arm. We also show that the Cetus system is confidently associated with the Triangulum/Pisces, Willka Yaku, and the recently discovered C-20 streams. The association with the ATLAS-Aliqa Uma stream is much weaker. All of these stellar debris are very metal-poor, comparable to the average metallicity of the southern Cetus stream with $[\mathrm{Fe/H}] = -2.17 \pm 0.20$. The estimated stellar mass of the Cetus progenitor is at least $10^{5.6}\,M_{\odot}$, compatible with Ursa Minor or Draco dwarf galaxies. The associated globular cluster with similar stellar mass, NGC 5824 very possibly was accreted in the same group infall. The multi-wrap Cetus stream is a perfect example of a dwarf galaxy that has undergone several periods of stripping, leaving behind debris at multiple locations in the halo. The full characterization of such systems is crucial to unravel the history of the assembly of the Milky Way, and importantly, to provide nearby fossils to study ancient low-mass dwarf galaxies.

Unified Astronomy Thesaurus concepts: Galactic archeology (2178); Stellar streams (2166); Dwarf galaxies (416); N-body simulations (1083)

1. Introduction

Low-mass dwarf galaxies are dark matter-dominated systems thought to play an important role in the hierarchical formation of Galactic dark matter halos. The search for the most extreme examples of these systems in the vicinity of the Milky Way has been transformed by the systematic mapping of the sky made possible by large panoptic surveys. In particular, the Sloan Digital Sky Survey (SDSS; York et al. 2000) led to the discovery of many new dwarf galaxies significantly fainter than previously known systems (e.g., Willman et al. 2005a, 2005b; Belokurov et al. 2006; Irwin et al. 2007; Koposov et al. 2008). This revolution, initiated with the SDSS, was continued through a series of similar surveys conducted in the last decade, including Pan-STARRS1 (PS1; Chambers et al. 2016) and the Dark Energy Survey (DES; The Dark Energy Survey Collaboration 2005). Trawling these data sets led to the discovery of tens of new faint dwarf galaxies that orbit the Milky Way (e.g., Bechtol et al. 2015; The DES Collaboration et al. 2015; Koposov et al. 2015; Laevens et al. 2015; Martin et al. 2015, and references within).

Low-luminosity dwarf galaxies, expected to inhabit the lowest-mass dark matter halos that can form stars (e.g., Bullock & Boylan-Kolchin 2017), garner a lot of interest as they are thought to be direct fossils from the very early universe (Bovill & Ricotti 2009). The faintest of all, with only 10^3–$10^5\,M_{\odot}$ in stars, are observed to have short star formation histories, limited to the first 1–2 Gyr after the big bang ($z \sim 5$; e.g., Brown et al. 2014), and have average metallicities $[\mathrm{Fe/H}] \lesssim -2$ (Simon 2019). Because of their relatively simple chemical enrichment history, the elemental abundances of stars from these systems are extremely sensitive to star-forming activities, the initial mass function, and neutron capture events (*s*- and *r*-process). These information is decoded using high-resolution (HR) spectra of stars in these ancient systems. However, the closest dwarf satellites remain $\sim$30 kpc away from us, which significantly limits the number of bright stars

amenable to high signal-to-noise HR-spectroscopic observations before the advent of 30 m telescopes.

On the other hand, the hierarchical formation that every galaxy undergoes means that numerous low-mass dwarf galaxies were accreted onto the Milky Way, and during their disruption, they left relics in the stellar halo (see, e.g., Johnston 1998; Bullock & Johnston 2005; Amorisco 2017; Monachesi et al. 2019). Identifying halo stars that previously belonged to the same low-mass dwarf galaxy would allow us to study their ancient progenitor with more detailed spectroscopic information than in current dwarf galaxies, as their stellar debris might extend to much closer distances. Thanks to the ESA/Gaia mission (Gaia Collaboration et al. 2016) discovering the very low surface brightness remnants of tidally disrupted low-mass dwarf galaxies is now an achievable goal. In synergy with the efforts designed to search for low-metallicity stars (e.g., Beers & Christlieb 2005; Starkenburg et al. 2017; Li et al. 2018), many studies have started to unveil the traces of low-metallicity accreted systems (Sestito et al. 2019, 2020; Wan et al. 2020; Yuan et al. 2020a, 2020b; Martin et al. 2022a, 2022b).

In parallel, the library of stellar debris is continuously increasing, including streams of globular cluster origins, detected based on their coherence in phase space (see, e.g., Malhan et al. 2018; Price-Whelan & Bonaca 2018; Bonaca et al. 2019; Ibata et al. 2019b, 2021; Li et al. 2022), and substructures of dwarf galaxy origins, identified from their clustering signatures in dynamical space (see, e.g., Helmi et al. 1999, 2018; Belokurov et al. 2018; Myeong et al. 2018a, 2019; Koppelman et al. 2019; Matsuno et al. 2019). A list of studies have shown that these disrupted stellar systems, together with globular clusters and chemically peculiar stars with halo orbits, can be grouped based on similar orbital properties, suggestive of their common origins (Myeong et al. 2018b, 2019; Roederer et al. 2018; Massari et al. 2019; Naidu et al. 2020; Yuan et al. 2020b; Bonaca et al. 2021; Gudin et al. 2021; Li et al. 2022; Limberg et al. 2021; Shank et al. 2022). Detailed abundance studies for these stellar debris have been made possible by HR-spectroscopic follow-up studies (Ji et al. 2020; Aguado et al. 2021a, 2021b; Gull et al. 2021; Matsuno et al. 2021), as well as by HR-spectroscopic surveys, such as the GALAH survey (Buder et al. 2022; Simpson et al. 2021).

In this work, we focus on the systematic search for members of a disrupted low-mass dwarf galaxy, the Cetus stream system, and assess its associations with several stellar relics that possibly share a common origin. A tailored *N*-body model is also used to interpret its stripping history. This is one of the few dwarf galaxy streams that preserve coherent structures in configuration space and allow us to decode their disruption history through modeling. The other two such systems include the textbook example of the Sagittarius (Sgr) stream (Mateo et al. 1996; Ibata et al. 2001; Majewski et al. 2003) with an extensive list of simulation studies (see, e.g., Law & Majewski 2010; Peñarrubia et al. 2010; Vera-Ciro & Helmi 2013; Dierickx & Loeb 2017; Vasiliev et al. 2021) and the LMS-1 from recent studies (Yuan et al. 2020a; Malhan et al. 2021). Ultimately, the list of confidently associated Cetus members should yield a sizable sample of stars to study the chemical evolution of a small and ancient dwarf galaxy.

The Cetus stream was first discovered by Newberg et al. (2009) using data from the SDSS and they suggested an association with the globular cluster NGC 5824 based on radial velocities. With the second data release of Gaia (Gaia Collaboration et al. 2018), Yuan et al. (2019, hereafter, Y19) identified ∼150 Cetus members by their clustering in kinematic space and confirmed the association with NGC 5824 based on the similarity of their orbits. They showed that Cetus is comprised of two parts on opposite sides of the Galactic disk where it is difficult to track its stars. Both parts of the stream have a mean metallicity $[\mathrm{Fe/H}] \approx -2$ with an intrinsic metallicity dispersion of 0.1–0.2 dex, suggesting its progenitor was a low-mass dwarf galaxy according to the stellar mass–metallicity relation (Kirby et al. 2013). Based on the more densely populated wrap identified in the Galactic South, Chang et al. (2020) performed an *N*-body model of the stream and predicted that about half of its members are distributed in the southern sky. In the model, the southern extension of the Cetus stream overlaps the location of the Palca stream discovered in the DES (Shipp et al. 2018), with a compatible distance. If this association is confirmed, it would extend the known length of Cetus by an additional ∼40°. The Southern Stellar Stream Spectroscopy Survey (S5; Li et al. 2019) reported observations of 25 Palca members in the field of the ATLAS-Aliqa-Uma (AAU) stream (Li et al. 2021), which overlaps Palca on the sky but with a perpendicular stream track. Most of the Palca members near AAU have kinematics consistent with the Cetus model (Li et al. 2022), as will be shown in detail in this study. This confirmation encourages us to search for more Cetus-Palca members in the southern sky.

To explore the southern hemisphere, where spectroscopic data is lacking, for extension of the Cetus stream we take advantage of the most up-to-date stream catalog derived with the `STREAMFINDER` algorithm (Malhan & Ibata 2018; Ibata et al. 2019b, 2021) as it does not require radial velocity measurements. The algorithm evaluates the probabilities of stars being in streams based on the similarity of their orbital properties with those of their neighbors. `STREAMFINDER` has proven hugely successful, with numerous new discoveries (Malhan et al. 2018), including the extended Phlegethon stream (Ibata et al. 2018), and the long sought-after stream of ω-Cen (Ibata et al. 2019a) predicted by simulations (see, e.g., Bekki & Freeman 2003; Mizutani et al. 2003; Ideta & Makino 2004; Tsuchiya et al. 2004). Using the newly released Gaia EDR3 and continuous optimizations of the search algorithms, the Milky Way's stream landscape has been recently updated (Ibata et al. 2021). The most recent `STREAMFINDER` catalog includes a search for wide streams, with which we detected the most nearby dwarf galaxy stream ($d \sim 20$ kpc), LMS-1 (Malhan et al. 2021). These streams are highly coherent in kinematic space, and therefore clean stream tracks can be revealed by exerting cuts on proper motion and significance, the latter of which quantifies the stream-like behavior.

In the case of the Cetus stream, it is known to be spatially separated, and diffusely distributed in phase space (Y19), which makes it difficult to implement clean membership filters with simple kinematic cuts. In order to select the most likely Cetus members, we fuse `STREAMFINDER` with another stream-searching algorithm, `StarGO` (Stars' Galactic Origins), developed from a totally different perspective (Yuan et al. 2018). The latter algorithm is a neural network based clustering tool, built on one of the most popular unsupervised learning algorithms, the self-organizing-map (SOM). Utilizing the power of SOM to store and visualize n-D data structures, a systematic group-identification procedure was developed to

search for streams and substructures clustered in dynamical space. The underlying assumption is that stars sharing the same origins preserve their clustering signatures in their orbital properties after they are stripped from their progenitor. StarGO has successfully led to the identification of the Cetus stream in Y19, the discovery of the LMS-1 structure (Yuan et al. 2020a), and a plethora of dynamically tagged groups (DTGs) in the nearby stellar halo (Yuan et al. 2020b).

Our strategy in the present contribution is to first obtain a sample of Gaia EDR3 stars that are likely to be in streams identified by STREAMFINDER, together with their orbital properties given their most likely orbits as derived by this algorithm. STREAMFINDER does not, however, link together stars that are part of the same stream. We therefore apply StarGO to the selected sample, and identify DTGs that have similar properties with the known Cetus stream. In the previous applications of StarGO, the dynamical parameters were derived from observational quantities, whereas, here, they are calculated from the predicted values of STREAMFINDER. This fusion of the two methods allows us to get the most likely candidate member list for the Cetus stream in the southern sky, where line-of-sight velocity information is largely missing. Further confirmation of the membership requires radial velocity measurements, as addressed below.

We describe the detailed detection procedure in Section 2. After we get the new member list for the Cetus system, the data used for member confirmation is shown in Section 3. The confirmed Cetus stream members and associated stellar debris are discussed in Section 4. The orbital properties of different Cetus components are compared to the current N-body model in Section 5. We then estimate the mass of the Cetus progenitor dwarf galaxy in Section 6. A discussion and conclusion are given in Section 7.

2. Algorithmic Detection of the Cetus Stream

2.1. The STREAMFINDER Sample

To search for the Cetus debris over the full sky, we first apply STREAMFINDER to the Gaia EDR3 catalog. The overall procedure for detecting this stream is similar to the one employed in Ibata et al. (2021); however, we made changes in some of the parameters so as to specifically search for Cetus. We use a fixed stellar population template of age = 12.5 Gyr and $[\mathrm{Fe/H}] = -2.2$ from the PAdova and Trieste Stellar Evolution Code (PARSEC) library (Bressan et al. 2012). We adopt a stream width of (Gaussian) dispersion 500 pc, and allow to search for neighbors in 10° along the orbit in a distance range from 10–100 kpc. For comparison, the standard STREAMFINDER run designed to search for thin and cold streams, uses a stream width of 50 pc, and a distance range of 1–30 kpc (Ibata et al. 2019b, 2021). All parameters in this work are motivated by the previous knowledge that we possess for the Cetus system from Y19, i.e., Cetus is a fairly wide stream, has distant members all the way to 50 kpc, and has a low average metallicity ($[\mathrm{Fe/H}] \approx -2.0$). The rest of the algorithm is set up to work as described in Ibata et al. (2021). It avoids the Galactic disk region ($|b| \leqslant 20°$) that is prohibitively expensive in computing time to explore, and scans through the heliocentric radial velocity space. Given the measured on-sky position, proper motion, and the assumed distance of a star, its trial orbits are calculated for a grid of radial velocities. The algorithm then evaluates the likelihood of this specific star being in a stream (see Equation (2) in Ibata et al. 2021). The radial velocity solution with the highest likelihood is selected and is used to calculate the significance that this star belongs to a stream.

In the rest of the paper, we restrict ourselves to stars with a significance $\geqslant 6\sigma$ (log-likelihood $\geqslant 19.8$). Note that this significance cut is lower than that used in previous STREAMFINDER studies: 7σ (Ibata et al. 2021) and 10σ (Malhan et al. 2021). The lower significance cut allows us to retain a generous sample (175,514 stars) while the following application of StarGO will help screen spurious members that could have made it into the sample.

2.2. Application of StarGO

The next step of the workflow is to apply StarGO to identify DTGs from the orbital properties of the sample stars, as inferred by STREAMFINDER. In particular, we focus on the space defined by the orbital energy, E, the orbit's angular momentum along the Galactic z direction, L_z, and the two parameters $\theta = \arctan(L_x/L_y)$ and $\phi = \arcsin(L_z/L)$, where L_x and L_y are the components of the angular momentum vector along the Galactic x and y directions, respectively. Although orbital poles change over time especially in an axisymmetric potential, the changes can remain coherent for a long period of time, and the clustering features of stars from a common origin are mainly preserved. This input space is similar to that used in the previous StarGO applications (Yuan et al. 2019, 2020a, 2020b); we only replace the total angular momentum by L_z in the current application. To enhance the signal from the Cetus stream, the sample is further culled by requiring $-45° \leqslant \theta \leqslant 0°$ from the full range of $[-90°, +90°]$, and orbital energy $E < 0$. These selections are based on the current knowledge (Yuan et al. 2019; Chang et al. 2020) that the orbit of the Cetus stream is close to polar, and centered on $\theta \approx -30°$ (prograde with an angle of 60° with respect to the Galactic z-axis). This yields a sample of 35,286 stars.

The first step of StarGO is to *feed* the sample to a 400×400 neural network, whose visualization is shown in Figure 1, panels (b) and (c). At each grid point of the 2D map, there is a neuron that carries a weight vector with the same dimension as the input vector (i.e., 4D). The neurons will learn the behavior of the input data set by iteratively updating their weight vectors, until convergence is reached. The learning algorithm is a self-organizing map (SOM), which preserves the topological structures of the n-D input data set and stores them on the 2D map (Kohonen 1982). The difference in weight vectors between neighboring neurons is denoted by a 400×400 matrix, $\boldsymbol{u}_{\mathrm{mtx}}$. Although the difference is calculated as the distance between neurons in the 4D weight vector space, the information in each dimension is preserved by their relative locations on SOM. Therefore, clustering algorithm based on SOM does not have the *curse of dimensionality* problem that traditional distance-based clustering methods have (Duch & Naud 1996), with similar distances between different pairs of input data. Compared to the density-based clustering methods, SOM can reveal clusters that have a variety of topologies that differ from a centrally distributed blob, such as a tire tube of linked data points in the n-D input space.

We are able to get the distribution of all the element u values from $\boldsymbol{u}_{\mathrm{mtx}}$, shown in Figure 1(a). Neurons with $u \leqslant u_{30\%}$ (30th percentile of the distribution of u) have similarities in weight vectors that lie in the top 30%. These are highlighted in white in

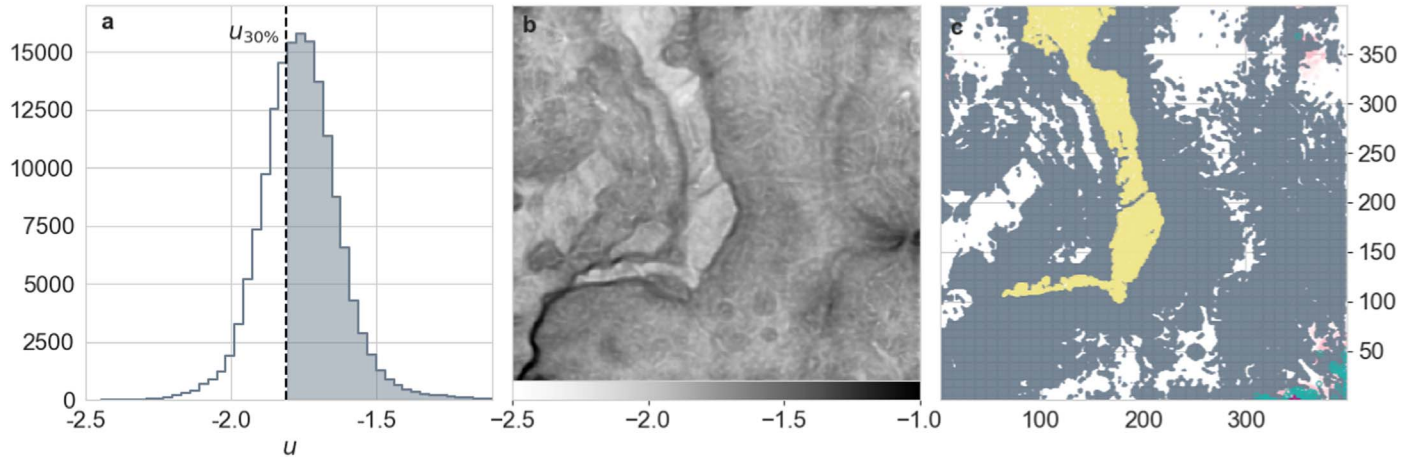

Figure 1. Training results from the application of StarGO to the selected STREAMFINDER catalog in the normalized space of (E, L_z, θ, ϕ). The (4D distances) differences in weight vectors between neighboring neurons are denoted by the u values, shown as the histogram in (a). The threshold for group identification is $u_{\rm thr} = u_{30\%}$, which defines the division line between the white and shaded areas under the curve. (b) The resulting self-organizing map (400 × 400 neuron network) color coded by the u values, where the relatively white patches correspond to the stars clustered in the input space. (c) Neighboring neurons with $u \geqslant u_{30\%}$ are colored in gray. At this threshold, two groups are identified in the khaki colored region. The Cetus members (green circles) identified from Y19 are mapped to the bottom-right corner (see Figure 2 for a zoom-in view).

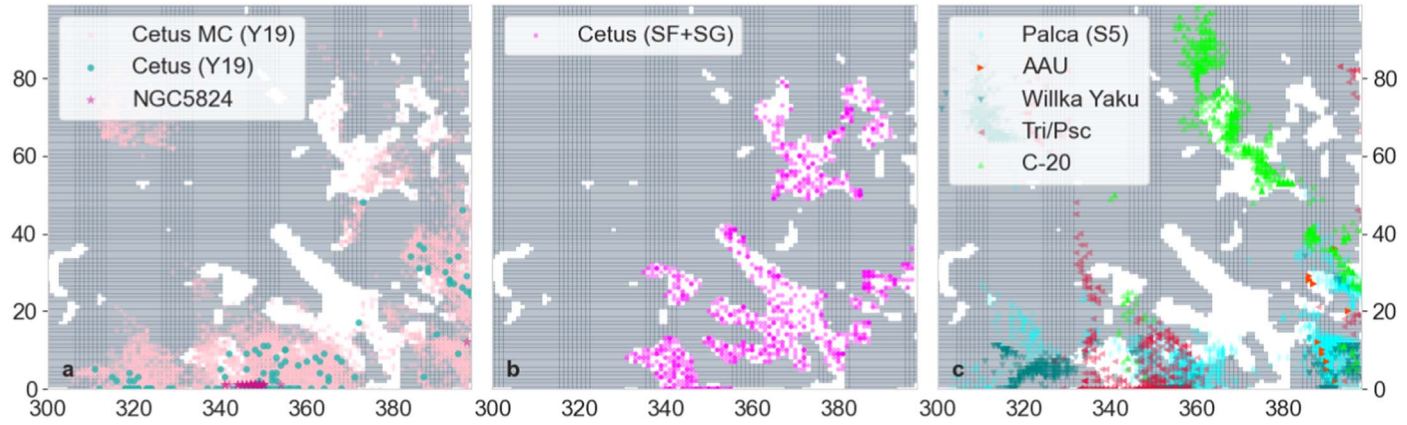

Figure 2. Zoom-in view of the SOM in the bottom-right corner of Figure 1, where the previous Cetus members from Y19 are mapped. The 130 Cetus members stars (green circles), all the MC realizations (100 for each) of the Cetus members (pink circles), and the MC realizations of NGC 5824 (violet star). (b) The DTGs are identified at $u_{\rm thr} = u_{30\%}$ in the Cetus region, and the stars from the STREAMFINDER sample associated with the Cetus DTGs are plotted by magenta circles. (c) The MC realizations of the 24 Palca members (cyan diamonds), 18 AAU members (orange right triangles), 11 Tri/Psc members (red left triangles), nine Willka Yaku members (dark green inverted triangles), and nine C-20 members (light green upper triangles) are mapped to SOM. Except for AAU, most of the realizations of the other stellar debris are located in the Cetus region.

panels (a) and (c), in contrast to the rest of the distribution, shown in gray. These neurons correspond to stars relatively clustered in the input space compared to the rest of the sample. We then create direct linkages between stars and neurons. This is done by finding the neuron that has the weight vector closest to the input vector of a given star, and this neuron is defined as the best matching unit (BMU). Through this step, stars mapped to the islands separated by the gray boundaries in panel (c) are defined as candidate groups at $u_{\rm thr} = u_{30\%}$. At each threshold value $u_{\rm thr}$, different candidate groups can be identified from a SOM. A candidate group is validated according to its estimated contamination rate, which will be discussed in detail in the next section.

2.3. Group Identification from Known Cetus Members

To isolate the parts of the SOM that correspond to likely Cetus members, we modified the group-identification procedure from Yuan et al. (2020b) by mapping the Cetus stream stars detected by Y19 to the SOM presented in the previous section. This allows us to use known Cetus members to guide group identification. We see that previously identified Cetus members from Y19, shown as green circles in Figure 1(c), cluster in the lower-right corner. We therefore focus on this region for group identification (see the zoom-in view of the SOM in Figure 2(a)). This is done by decreasing $u_{\rm thr}$ until isolated islands emerge from the gray boundary. We detect a group of islands at $u_{\rm thr} = u_{30\%}$ (magenta patches in Figure 2(b)). At the same threshold, two large DTGs are identified in the middle of the SOM (yellow patches in Figure 1(c)), which are the most obvious structures revealed in (b). The on-sky projection of these DTGs immediately show that they correspond to the Sgr stream (see yellow scatter in Figure 3). On the contrary, the Cetus DTGs (magenta points in panel (b)) overlap and extend the known Cetus stream (filled green squares in panel (a)). Both the identified Sgr and Cetus streams have two parts separated by the Galactic plane, since we avoid the disk region ($|b| \leqslant 20°$).

As with the previous exploration of the STREAMFINDER catalog (see Figure 5 in Ibata et al. 2019b), we find a broad

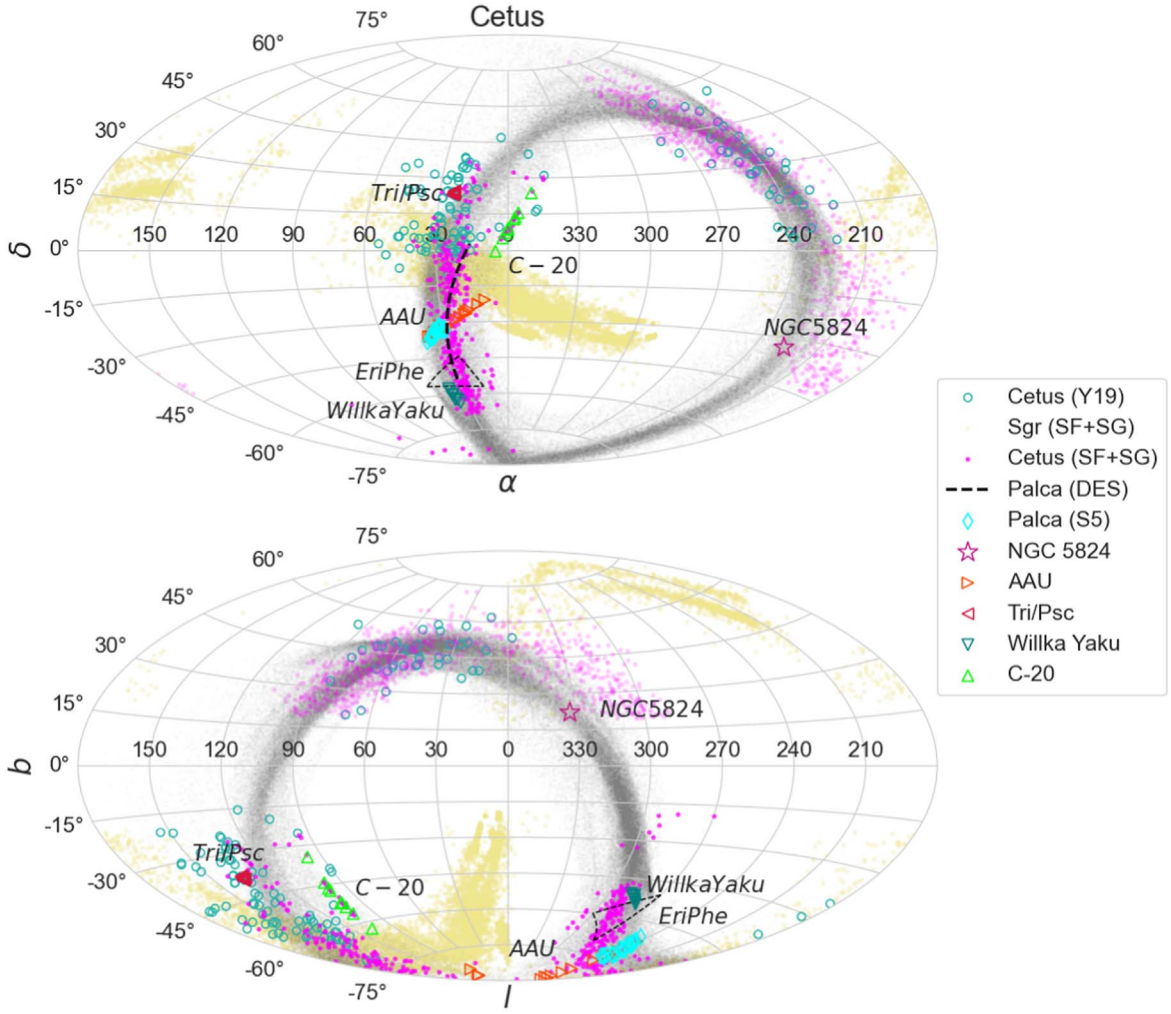

Figure 3. On-sky projection of the Cetus system in the Equatorial (upper) and Galactic (lower) coordinates. The Cetus stream from Y19 is denoted by open green circles. The Sgr DTGs identified in this work are shown as khaki colored circles. The *N*-body model of the Cetus stream from Chang et al. (2020) is plotted as gray scatter in the background. The Cetus DTGs identified at the same $u_{\rm thr}$ are denoted as solid magenta circles in the south, and as transparent magenta circles in the north, where it is heavily contaminated. The track of Palca from DES is denoted by the black dashed line. The possible associated debris are represented by a violet star (NGC 5824), cyan diamonds (Palca), red left-pointing triangles (Tri/Psc), dark green inverted triangles (Willka Yaku), and light green triangles (C-20). AAU (orange right-pointing triangles) is located in the footprint of the southern Cetus, but its association is much weaker compared to the other debris. The region of the EriPhe overdensity is shown as the black dashed triangle.

feature of unknown origin in the region $-60^\circ < l < 60^\circ$ and $-45^\circ < b < 45^\circ$. In the present study, this feature is present well beyond 10 kpc, which was the distance upper limit in the maps of Ibata et al. (2019b). This coherent structure surrounds the Milky Way center and reaches as far as 30 kpc, which forms a significant contaminating population for stream identification. Note that the northern Cetus largely overlaps with the footprint of this structure. Therefore, we expect the northern Cetus members to be more contaminated by this halo population, which can be seen from their more diffuse distribution compared to the southern counterpart. Due to this reason, we divide all the DTG members into the northern and southern sets, and estimate the contamination fraction ($\mathcal{F}_c$) and significance for these two sets separately.

To validate the DTGs and assess their contamination levels, we generate a mock sample that has the same distribution as the training sample in the input space, but contains no correlations between the input dimensions from streams. In other words, we reshuffle the training sample $\mathcal{T}$ in each dimension of the input space, yielding a shuffled mock sample $\mathcal{M}$. In doing so, we wash out the correlations that are intrinsically present in the DTGs of the input space and $\mathcal{M}$ can be used to estimate the expected contamination from a smooth halo sample. Compared to the procedure described in Yuan et al. (2020b), the two sets of Cetus DTGs (northern and southern) are combined into one group, and similarly for the Sgr DTGs. For a given set $\mathcal{S}$ of n stars in one group identified from the training sample ($\mathcal{T}$) of N stars in the same set, we apply the following steps:

1. Find the best matching unit (neuron), BMU, for every star of $\mathcal{M}$ on the trained neuron map, and obtain the $n_{\mathcal{M}}$ stars associated with set $\mathcal{S}$. The probability of stars from $\mathcal{M}$ to be identified in $\mathcal{S}$ is $p_{\mathcal{M}} = n_{\mathcal{M}}/N_{\mathcal{M}}$.
2. Calculate the binomial probability $\mathcal{P}$ of detecting a set with more than n stars from the total sample of N stars, given probability p. If $1 - \mathcal{P} \geqslant 99.73\%$, the significance of $\mathcal{S}$ is greater than 3σ, and we consider it as a potentially detected set.
3. If $\mathcal{S}$ is a potentially detected set, we estimate the contamination fraction from $\mathcal{M}$, which is defined as $\mathcal{F}_c = p_{\mathcal{M}}/p$.

Table 1
Stellar Stream Systems

Cetus				Sagittarius			
		n	Contamination			n	Contamination
Set	North	829	36%	Set	North	1422	35%
	South	359	13%		South	7074	27%
		n ($n_{\rm tot}$)	Confidence				Confidence
Part	Cetus (Y19)	104 (130)	30%	Associate	Arp2		100%
	Cetus (SF+SG; RV)	41 (44)	35%		Terzan8		100%
	Palca (S5)	23 (24)	15%		Pal12		100%
Associate	NGC 5824		86%		M54		99%
	C-20	9 (9)	36%		Whiting1		95%
	Tri/Psc	9 (11)	19%		Terzan7		42%
	Willka Yaku	9 (9)	13%		NGC 2419		10%
					Pal2		5%
Non-associate	AAU	2 (17)	2%	Non-associate	Pal4		1%

Note. The northern and southern sets of both streams identified in this work are listed in the first part of the table. The Cetus stream identified in different studies are shown in the second part of the table for the Cetus columns. All the candidate associated structures in this study are listed, and divided into the valid ($\mathcal{C} \geqslant 5\%$) and nonvalid categories based on their confidence values.

The two sets in the Sgr and Cetus groups all have significance values greater than 3σ, and their contamination fractions are listed in Table 1. As expected, the northern Cetus set is much more contaminated ($\mathcal{F}_c = 36\%$) than the southern set ($\mathcal{F}_c = 13\%$) because the coherent halo structure mentioned above heavily overlaps the northern Cetus set, and has a significant contribution to the re-shuffled sample. The two Sgr sets have similar contamination levels, with $\mathcal{F}_c = 35\%$ (N) and 27% (S), and exhibit clear features of the stream from their on-sky projections, as shown in Figure 3. Based on the comparisons of $\mathcal{F}_c$ between the different sets, we are highly confident about the quality of the southern Cetus set, while the northern Cetus set is more prone to biases because of the contamination. We therefore mainly focus on the southern part of the Cetus stream in the rest of the analysis.

3. Data

3.1. Spectroscopic Data

The list of southern Cetus members was built without any radial velocity information, which gives us the opportunity to check the reliability of these members by gathering radial velocities from public archives and dedicated observations. We are first able to collect velocity measurements for 23 stars by crossmatching with public spectroscopic surveys. We find that 11 stars in our sample were also observed in the SDSS/SEGUE survey (Yanny et al. 2009), three have velocities in LAMOST DR7 (Cui et al. 2012; Zhao et al. 2012), and nine stars are in the S5 DR1 (Li et al. 2019).

To complement this data set we obtained radial velocities from VLT/UVES spectra observed in 2021 May 18–21 and 2021 October 23–24 via programs 0105.B-0235(A) (PI: Ibata) and 0108.B-0431(A) (PI: Yuan). In total, we obtained spectra for four member stars of the C-20 stream (Ibata et al. 2021) in 2021 May (which we will show below is a cold stream likely associated to Cetus), along with five additional members and 21 Cetus stream members in October. The UVES spectrograph was set up with the DIC2 dichroic beamsplitter in the wavelength range of "437+760," which covers 3730–4990 and 5650–9460 Å. To increase the efficiency of our short exposures of 10–20 minutes, we used the 2×2 pixel binning readout mode and a $1''$ slit, yielding a resolution of $R \sim 40{,}000$. All of the spectra were extracted and wavelength calibrated with the `esorefex` pipeline.[12] To measure the radial velocities of the observed stars, we used the `fxcor` algorithm in IRAF, cross correlating against the spectrum of the radial velocity standard star HD 182572. The metallicities of the three brightest C-20 stars are analyzed with `MyGIsFOS` (see Sbordone et al. 2014, for more detail).

3.2. Distance Estimation

For all Cetus members detected in this work, we infer their distances using a Bayesian approach following Sestito et al. (2019, 2020). Very briefly, we calculate the probability distribution function (PDF) of the heliocentric distance by merging the Gaia EDR3 photometry (G, BP, and RP) and parallax ϖ with a prior on the Galactic stellar density profile and with `PARSEC` isochrones (Bressan et al. 2012). The isochrones are selected to be very metal-poor ([Fe/H] $= -2.0$) and with an age of 12 Gyr, in line with the expected properties of an old, low-mass dwarf galaxy like Cetus. Note that the differences between the isochrones used in the `STREAMFINDER` algorithm and the distance estimation here are negligible compared to the uncertainties of the photometric measurements. This isochrone is used throughout this work. Gaia EDR3 photometry was de-reddened using the dust map from Schlegel et al. (1998) corrected by Schlafly & Finkbeiner (2011), and updated for the Gaia passbands.[13] For many objects in our sample, the Gaia parallax values are very uncertain (e.g., $\delta_\varpi/\varpi \geqslant 20\%$, or $\varpi < 0$ mas), which usually implies a large distance and stars that are likely to be associated with a distant halo structure. We therefore assume that all stars are giants, which means that, in cases where the PDF of a star displays both a dwarf and a giant solution, the farthest one is adopted.

[12] https://www.eso.org/sci/software/esoreflex/
[13] $A_G/A_V = 0.86117$, $A_{BP}/A_V = 1.06126$, and $A_{RP}/A_V = 0.64753$.

There are several distant streams that will be shown to be likely associated to the Cetus system. Since they are in deep photometric surveys, we decide to take the distances estimated from their photometry. For the Palca stream discovered from the DES photometry (Shipp et al. 2018), we estimate its distances as the average of its six blue-horizontal-branch (BHB) members (33.2 kpc) following the approach presented in Deason et al. (2011). Compared to the distance modulus estimation based on the DES photometry (36 kpc, Shipp et al. 2018) and the averaged BHB distance estimated from Li et al. (2022, $d = 36.3$ kpc,), the differences among these estimates are within 10%.

4. Cetus Debris System

4.1. Original and Expanded Cetus

Combining all Cetus DTGs associated with the magenta area in the SOM shown in Figure 2(b) there are 359 southern members, 44 of which have radial velocity measurements from spectroscopic surveys and follow-up studies. For each given star, we generate 100 Monte Carlo (MC) realizations of dynamical parameters based on observational uncertainties in 6D space using AGAMA (Vasiliev 2019) with the Milky Way potential from McMillan (2017). We then find the corresponding BMU for each realization on the trained neuron map. The valid realizations are those associated to the Cetus DTGs (magenta patches in Figure 2(b)), shown as magenta circles in the input space (see Figure 4(a), (b)). 41 out of the 44 candidates that have radial velocity measurements can be associated with the Cetus DTG through with the MC procedure and thus are considered valid members, with an overall confidence of 35% (35 out of 100 realizations are re-associated). Similarly, the valid realizations drawn from the member list of Y19 are plotted as green circles and overlap the region of the new members. We then derive the mean and dispersion of all the confirmed Cetus members in L_z and E using the formalism of Martin et al. (2018) by taking into account the observational uncertainties in the radial velocities, proper motions, and distances. The derived values are plotted as the red symbols in Figure 4(a), (c), which agree with the values derived directly from the Cetus model from Chang et al. (2020) shown as the dark blue symbol.

The probability of a given member being associated with Cetus is the number ratio of the valid associations out of 100 MC realizations, which can be re-associated to the Cetus DTGs on the neuron map. The confidence level ($\mathcal{C}$) is defined as the average probabilities of valid associations for re-associated members. With this definition, 104 of 130 Cetus members listed by Y19 are identified as members (with nonzero probabilities), with $\mathcal{C} = 30\%$, denoted as the confidence in Table 1. The fact that the training samples are different in these two studies largely explains why some of the stars previously identified as members by Y19 are not valid realizations here. Every training set results in a unique SOM, for which the identified groups will not be entirely identical. The results depend on the training set, which in this study is generated from the predicted orbits based on STREAMFINDER.

We also emphasize that the $\mathcal{C}$ values listed here are indicative as large uncertainties; for instance, the more distant or fainter structures will lead to low values of $\mathcal{C}$. As such, $\mathcal{C}$ reflects both the accuracy of the orbital parameters and of the association itself and should not simply be taken as a direct evaluation of the intrinsic strength of an association. In this context, we find that all associates of the Sgr stream with $\mathcal{C} \geqslant 5\%$ correspond to known members of the stream (Bellazzini et al. 2020), using the updated proper motion measurements from Vasiliev & Baumgardt (2021). We therefore also use this threshold to isolate Cetus associates of interest. Except for the AAU stream, the other associates are considered as valid with $\mathcal{C}$ values listed in Table 1, including NGC 5824 as a highly confident one ($\mathcal{C} = 86\%$).

4.2. Palca and Atlas-Aliqa Uma and Eridanus-Phoenix

We can immediately see from the on-sky projection of the Cetus system shown in Figure 3 that the new southern extent of Cetus (magenta circles) connects with the previously known Cetus stream (green circles), and overlaps with the Palca stream track (dashed lines) from the DES (Shipp et al. 2018). The Palca stream has a fairly large width, and extends over 60°, almost reaching the edge of the DES survey at $\delta = -60°$. The potential connection between the Palca and Cetus streams was already discussed by Chang et al. (2020) and Li et al. (2022). Using the 24 Palca members with radial velocity measurements from S5 (cyan diamonds in Figure 3) in the field of AAU (Li et al. 2021), we apply the technique described in Section 4.1 to quantify the confidence of their association. It is clear that most of the Palca stars are located in the region of the Cetus DTGs in the zoom-in view of the SOM in Figure 1(c). In total, 23 out of 24 Palca members are identified to be associated with the Cetus DTGs, with an average confidence (probability) of 15% (see Table 1), after assigning an overly generous 20% uncertainty on this distance estimates we infer for the Palca stars (see Section 3.2). From the input space, the valid Palca realizations are located well within the region defined by the Cetus members (see Figure 4(c), (d)). A more detailed comparison between the Palca stream and the extent of the Cetus stream detected in this work is presented in Section 5.

As shown by Li et al. (2022), the AAU and Palca streams overlap each other in the (L_z, E) space, with a slight difference in the longitudinal angle of orbital poles (i.e., ϕ). This is consistent with this study, where most of the AAU realizations (maroon right-pointing triangles) are not mapped in the zoom-in Cetus region in Figure 2(c). There are only three out of 100 realizations that are associated with the Cetus DTGs, as shown in Figure 4. Their association has confidence $\mathcal{C} = 2\%$, and is considered as invalid based on the threshold of valid association defined in this study (see details in Section 4.1).

Among the southern stellar structures discovered in the DES, there is an overdensity, Eridanus-Phoenix (EriPhe) centered at $l \approx 285°$, $b \approx -60°$ (Li et al. 2016). We show it is right in the footprint of the southern Cetus, denoted by the dashed black triangle in Figure 3. There are no spectroscopic follow-up observations of the EriPhe members. However, Chang et al. (2020) predicted its possible association with the Cetus stream because the simulated stream covers the distance range of EriPhe ($d \approx 16$ kpc) in the same sky area. In this work, the southern Cetus members detected in the region of EriPhe have similar distances, which further strengthen this association (see details in Section 5.2). Note that this is one possible scenario for the origin of EriPhe, although other scenarios are also discussed in Li et al. (2016) and Donlon et al. (2020), which is before the discovery of the southern Cetus stream.

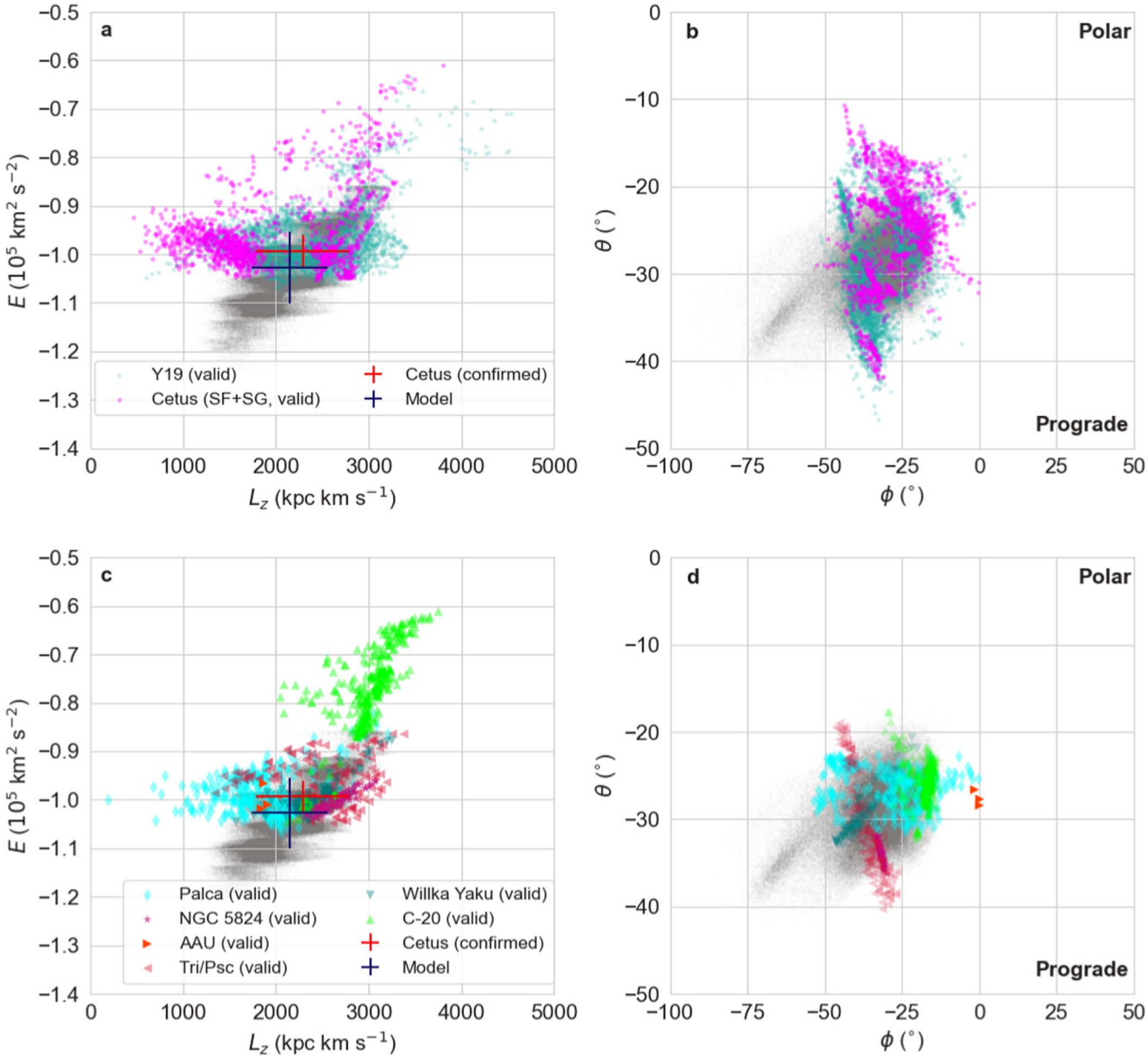

Figure 4. Valid MC realizations of the Cetus members with radial velocity measurements that are re-associated with the Cetus DTGs in Figure 2(b) are plotted in the input space (L_z, E) shown in (a) and (c), and (θ, ϕ) shown in (b) and (d), with the same color coding as Figure 2. θ and ϕ represent the two angles of the angular momentum vector, where negative θ corresponds to a prograde orbit. The existing and new Cetus members overlap with each other in (a), (b), as well as with the Cetus model shown as gray scatter in the background. The red symbol represents the mean and intrinsic dispersion of L_z and E from all the confirmed Cetus members, which agree with the values derived from the Cetus model shown as dark blue symbol. The Cetus members have orbital poles centered around $\theta = -30°$, i.e., 60° w.r.t the Galactic z. The valid realizations of NGC 5824, the Palca members, the Tri/Psc members, the Willka Yaku members, and the C-20 members are heavily overlapped in the Cetus region, whereas there are few valid realizations of the AAU members.

4.3. Triangulum/Pisces and Willka Yaku

Besides the kinematically hot Palca stream, there are three cold streams (Tri/Psc; Bonaca et al. 2012; Martin et al. 2013), Turbio, and Willka Yaku (Shipp et al. 2018) that are suggested to be associated with the Cetus stream by Bonaca et al. (2021). Among them, Tri/Psc and Willka Yaku are shown to be very close to NGC 5824 in phase space by Li et al. (2022), who claims that they likely came from the same group infall. Here, we use the Martin et al. (2013) member list of Pisces stars from SDSS DR8 to quantify the confidence of this association. We take the distance estimated from the stream's MSTO as seen in the PAndAS survey ($d \sim 27$ kpc Martin et al. 2014), and assume an uncertainty of 20%. The analysis yields $\mathcal{C} = 19\%$ for an association to the Cetus system, indicating a strong association.

For the Willka Yaku stream, we take the distance estimate ($d = 36.3$ kpc), and radial velocity measurements of its nine members from Li et al. (2022). The resulting confidence $\mathcal{C} = 13\%$ is similar to that of the Palca stream. For this stream as well, we reach the conclusion that it is confidently associated with the Cetus system.

4.4. C-20

In addition to possible associations already listed in previous studies, we notice a thin stream-like track from the southern Cetus members, at $\alpha \sim 0°$, $0° \lesssim \delta \lesssim 30°$ in Figure 3. This

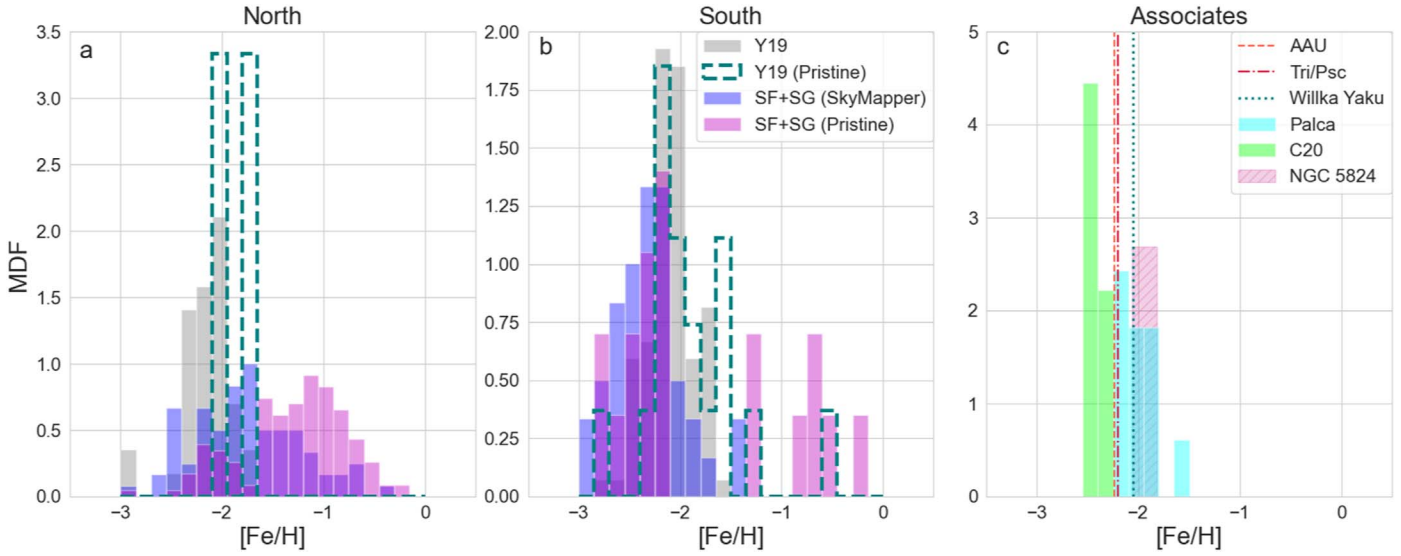

Figure 5. MDFs of the Cetus system from different survey data and spectroscopic follow-up studies. (a) The MDFs of the southern Cetus: the spectroscopic metallicities from LAMOST K Giants and SDSS BHBs for Y19 members (gray); the Pristine metallicities for Y19 members (dark green dashed line); the metallicities of members identified in this work by crossmatching with Pristine (magenta) and SkyMapper DR2 (blue). The four samples are all consistent, and gives an average $[Fe/H] = -2.1 \pm 0.2$. The northern Cetus members from Y19 are very metal-poor, whereas the members in this work have a wide MDF and cover the metal-rich regime in panel (b), indicating that they are heavily contaminated in the STREAMFINDER catalog. (c) The metallicities of the stellar debris possibly associated with the Cetus system: NGC 5824 (violet hatched bar and dashed lines); Palca (cyan histogram); C-20 (light green histogram); Tri/Psc (red dashed–dotted line); Willka Yaku (dark green dotted line); and AAU (orange dashed line) is not strongly associated with the Cetus system.

stream track coincides with the C-20 stream discovered by Ibata et al. (2021) and is relatively thin and cold compared to the Cetus stream. There are 14 C-20 stars in common with the Cetus member list. We obtained accurate velocity measurements for nine of those C-20 stars, which allows us to determine an association between the two structures at relatively high confidence ($\mathcal{C} = 36\%$). This is visible in the mappings of the MC realizations of these nine C-20 stars (light green triangles in Figure 1(c)), most of which are located in one of the Cetus DTGs. Consistently, the valid realizations of the C-20 stars heavily overlap with the Cetus members in the input space (see Figure 4(c), (d)).

4.5. Metallicities of the Different Components

We are able to compare the metallicities of all Cetus components and possible associations by crossmatching with data from different surveys. Figures 5(a) and (b) show the metallicity distribution function (MDF) of the Cetus members from Y19 and of the new members in this study, divided between the northern and southern sets. The MDF in Y19 from LAMOST K Giants and SDSS BHBs represented by the gray histograms and give an average $[Fe/H] = -2.2$ (north) and -2.3 (south). For those southern members also present within the footprint of the Pristine survey (Starkenburg et al. 2017), we rely on the photometric metallicities of this survey, based on narrow-band CaHK photometry. From the member list detected in this study, there are 154 northern stars and 20 southern ones in the Pristine survey, the MDFs of which are shown as magenta histograms in Figures 5 (a) and (b). The southern set has an average $[Fe/H] = -1.9$, and 13 members are very metal-poor (VMP; $[Fe/H] \leqslant -2$). On the other hand, the northern MDF has a bimodal distribution, which clearly shows a large source of metal-rich stars that are likely contaminants (see the discussion in Section 2.3). Similarly, using the photometric metallicities derived from SkyMapper DR2 data (Huang et al. 2021, 2022), the northern set shows an extended distribution, and the southern MDF exhibits a tight distribution with an average $[Fe/H] = -2.3$ shown as blue histograms. There are 35 out of 41 stars that are VMP in the southern set. In summary, the average metallicity of the southern Cetus is $[Fe/H] = -2.1 \pm 0.2$ from the two photometric data sets above.[14] Note that the 21 Cetus stars observed by VLT/UVES are chosen from the southern members with photometric metallicities below -2. The detailed spectroscopic analysis of element abundances will be presented in the future work.[15]

All the new structures we associate with Cetus based on the exploration of the SOM have average metallicities that are in agreement with these values. We show the metallicity of all associated debris in Figure 5(c). The MDF of the 23 Palca members (cyan histogram) has an average $[Fe/H] = -2.02 \pm 0.04$ from Li et al. (2022). The average metallicities of NGC 5824 is $[Fe/H] = -1.94 \pm 0.12$ (violet hatched bar) from Roederer et al. (2016), similar to -2.11 ± 0.01 from Mucciarelli et al. (2018). The average metallicity of Tri/Psc is $[Fe/H] = -2.2 \pm 0.3$ from SDSS DR8 spectroscopic data. Willka Yaku has an average metallicity $[Fe/H] = -2.05 \pm 0.07$ from S5 (Li et al. 2022). The metallicities of three C-20 stars that have been derived from the VLT/UVES spectra are denoted by the light green histogram, with an average $[Fe/H] = -2.44$. These two strong associates are both very metal-poor, consistent with the mean metallicity of the southern Cetus members. Although the association between the Cetus and the AAU streams is much less obvious, we note that the

[14] Before doing this average, we checked that the offset between Pristine and SkyMapper DR2 metallicities is small (0.07 dex) in the metal-poor regime ($[Fe/H] \leqslant -1.5$) from the cross-matched sample.

[15] A preliminary analysis of the iron abundance of two of the stars, Cetus23 ($[Fe/H] = -2.12 \pm 0.06$) and Cetus24 ($[Fe/H] = -1.96 \pm 0.09$) confirms their good agreement with the photometric metallicities ($[Fe/H] = -2.4 \pm 0.2$ and -1.8 ± 0.2, respectively) and the mean metallicity calculated above.

metallicity of the latter is also compatible, with an average $[Fe/H] = -2.24 \pm 0.02$ according to Li et al. (2021).

5. Comparison with the Cetus Model

We now compare the orbital properties of different Cetus components with simulations. Based on the previously detected Cetus stream in the northern sky, Chang et al. (2020) explored a range of initial conditions for the progenitor and found a favorable model that can match the morphology and features of the entire stream as seen in the (b, d, v_{gsr}) space. This model is represented by the small light gray points in Figure 6. In brief, the system has undergone a very long period of tidal stripping (8 orbital periods, ~5 Gyr), and left multiple wraps in the form of both trailing and leading arms. In order to compare the new findings with the N-body model, we unfold the simulated stream in the space of orbital phase and distance, (Ψ, r), as done by Chang et al. (2020) and shown in Figure 6(a). Here Ψ is the angle between the star and the progenitor's center with respect to the Milky Way center, and r denotes the Galactocentric distance. The center of the disrupted Cetus progenitor from the model is currently located at (0°, 20 kpc). We highlight the part of the streams in the Galactic south with different colors in Figure 6(a), and name the wrap closest to the center as L1 (yellow) in the leading arm ($\Psi \geqslant 0°$), T1 (orange) and T2 (light purple) in the trailing arm ($\Psi \leqslant 0°$), respectively.

The Cetus stream previously identified by Y19 is plotted in Figures 6(b) and (c). The southern members are separated into two clumps in (b, v_{gsr}), with opposite signs in v_{gsr} (negative velocities represented by green circles in panel (b), and positive velocities as pink circles in panel (c)). These two clumps are the most densely populated structures in the previous findings and clearly have different gradients in both d and v_{gsr} as a function of b. In order to reproduce these features in the model, the center of the disrupted system (black cross) does not overlap the associated globular cluster NGC 5824 (purple star) (see detailed discussions in Chang et al. 2020). We see that the globular cluster is located in the wrap stripped earlier than L1 in the leading arm. Although the predicted center might shift based on the new findings, the relative location of these wraps along the orbit remain the same.

5.1. Cetus-Palca Wrap

In panel (b), we plot the southern extent of the Cetus stream beyond 30 kpc (blue dots) that are detected in this work. In this relatively distant group with an average distance of 40 kpc, there are 26 stars that have radial velocity measurements. These are represented by the black and blue circles in the two panels of (b). The Palca members (cyan diamonds Li et al. 2021) have similar distances and radial velocities compared to the members at $b = -70°$. To show the orbit of this distant group, we adopt the orbit-sampling procedure instead of orbit-fitting because the latter would have been a poor approximation for such streams that are dynamically hot and physically broad. We use the phase-space information of the 26 stars with velocity measurements to constrain its orbit. The orbit of each member is obtained from 200 samplings of the observational uncertainties in proper motion, radial velocity, and distance. The averaged orbit from the samplings of the 26 members is denoted by the light blue dashed–dotted line. It has similar gradient as the previous Cetus component with negative v_{gsr} and aligns very well with the T1 wrap (orange). We therefore conclude that this distant group is the Palca stream discovered in the DES (Shipp et al. 2018) and is the southern extent of the Cetus stream with negative v_{gsr}, previously identified in the northern sky by Y19. The best-fit orbit (turquoise dashed line) of the Willka Yaku stream located at $b = -53°$ (red left-pointing triangle) is in line with the Palca orbit. We name this entire stream structure in the Galactic south as the Cetus-Palca stream wrap, and its part in the southern sky as the Palca wrap.

5.2. Cetus-New Wrap

In Figure 6(c), the southern Cetus members (magenta dots) at smaller distance ($d \approx 18$ kpc) form a clear stream track in the (b, d) space. Although this closer group is located in the same region as the Palca wrap on the sky, it is clearly a new wrap because it spreads over a different distance range and has a distinct gradient in (b, d). Its averaged orbit from sampling 18 members with velocity measurements (magenta circles) is shown as the purple dashed–dotted line. We find that the new wrap is the southern extension of the previously detected Cetus with positive v_{gsr} and closely follows the T2 wrap from the model (light purple). The EriPhe overdensity (black diamond) sits well within the southern wrap with similar distance. The Tri/Psc stream (red left-pointing triangles) resides among the Cetus members at $b \approx -38°$, and its best-fit orbit (pink dashed line) aligns closely with the orbit of the new wrap. We refer to the whole stream structure as the Cetus-New stream wrap, and its part in the southern sky as the new southern wrap. The Cetus-New wrap is the closest and densest wrap; thus, we estimate the properties of the Cetus stream according to this wrap. By applying the formalism of Martin et al. (2018), the stream width is estimated to be $5° \pm 0.^{\circ}3$ equivalent to the maximum width of ~1.6 kpc at the average distance of 18 kpc. The velocity dispersion is 12 ± 3 km s^{-1} based on the 15 members with radial velocity measurements.

5.3. C-20 Wrap

The best-fit orbit of C-20 is represented by the green dashed–dotted line in Figure 6(d). It is clear that its orbit has a different track from that of Cetus-Palca (T1) and the Cetus-New wrap (T2). The closest wrap of the Cetus model to C-20 is L1 (yellow) in the region with $b < 0°$ and $\delta > -40°$. L1 follows the stream track of C-20 in (b, v_{gsr}) but has a distance offset of about 10 kpc in distance. Interestingly, the orbit of C-20 comes across the AAU stream in both spaces. The best-fit orbit of AAU is shown as the orange dashed lines and they also agree with L1 in the observed region of the sky.

5.4. Proper Motion

We further investigate the correspondence between the different Cetus components and the simulated stream wraps from the Cetus model in proper motion space. In Figures 7(a) and (c), the Cetus-Palca wrap spreads from $\delta = 40°$ to $\delta = -60°$, and is made of the previously detected Cetus stream with negative v_{gsr}, the Palca wrap defined in this work, the Palca and the Willka Yaku streams from S5 (Li et al. 2021). The first wrap in the trailing arm (T1; orange) aligns very well with the entire stream track, as well as with the averaged sampling orbit of the Palca wrap (light blue dashed–dotted lines). The deviation from the sampling orbit occurs at $\delta > 15°$, which is likely due to the lack of members with radial velocity information in the region.

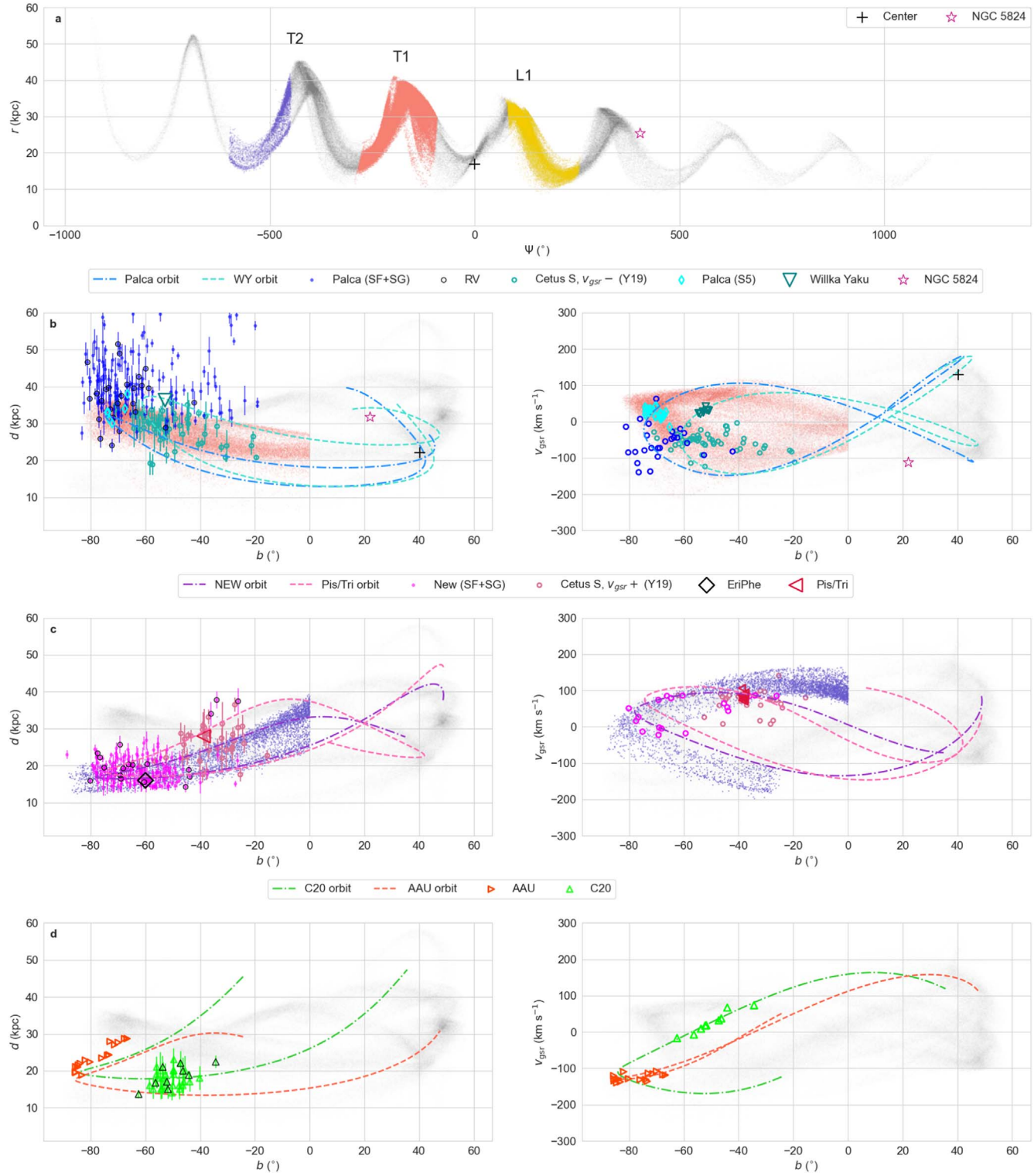

Figure 6. Comparisons of the Cetus debris with the stream model from Chang et al. (2020) in the (b, d, $v_{\rm gsr}$) space. (a) The entire simulated stream (gray scatter) is unfolded along the azimuthal angle Ψ and shown in the space of (Ψ, r). The three wraps in the leading and trailing arms closest to the center of the disrupted progenitor are L1 (yellow), T1 (orange), T2 (light purple), and only the segments of the wraps entering the sky region of the observed streams are colored. (b) The Cetus-Palca wrap is made of the northern Cetus with negative $v_{\rm gsr}$ (green circles), the Palca wrap (blue points), including the Palca members in S5 (cyan diamonds). The entire structure follows T1 (orange), as well as its sampling orbit (light blue dashed–dotted line). The best-fit orbit (turquoise dashed line) of the Willka Yaku stream (dark green inverted triangles) are in line with the Cetus-Palca wrap. (c) The Cetus-New wrap is composed of the northern Cetus with positive $v_{\rm gsr}$ (pink circles), the new southern wrap (magenta dots), which follows T2 (light purple), as well as its sampling orbit (purple dashed–dotted line). The Tri/Psc stream resides in the northern members, with its best-fit orbit (pink dashed line) aligned with the new wrap. The EriPhe overdensity (black diamond) has the same distance as the new southern members at $b = -60°$. (d) The C-20 stream (best-fit orbit, green dashed–dotted line), members (light green triangles) and the AAU stream (best-fit orbit, orange), and members (orange right-pointing triangles) mainly agree with L1 (yellow), despite some offsets in distances.

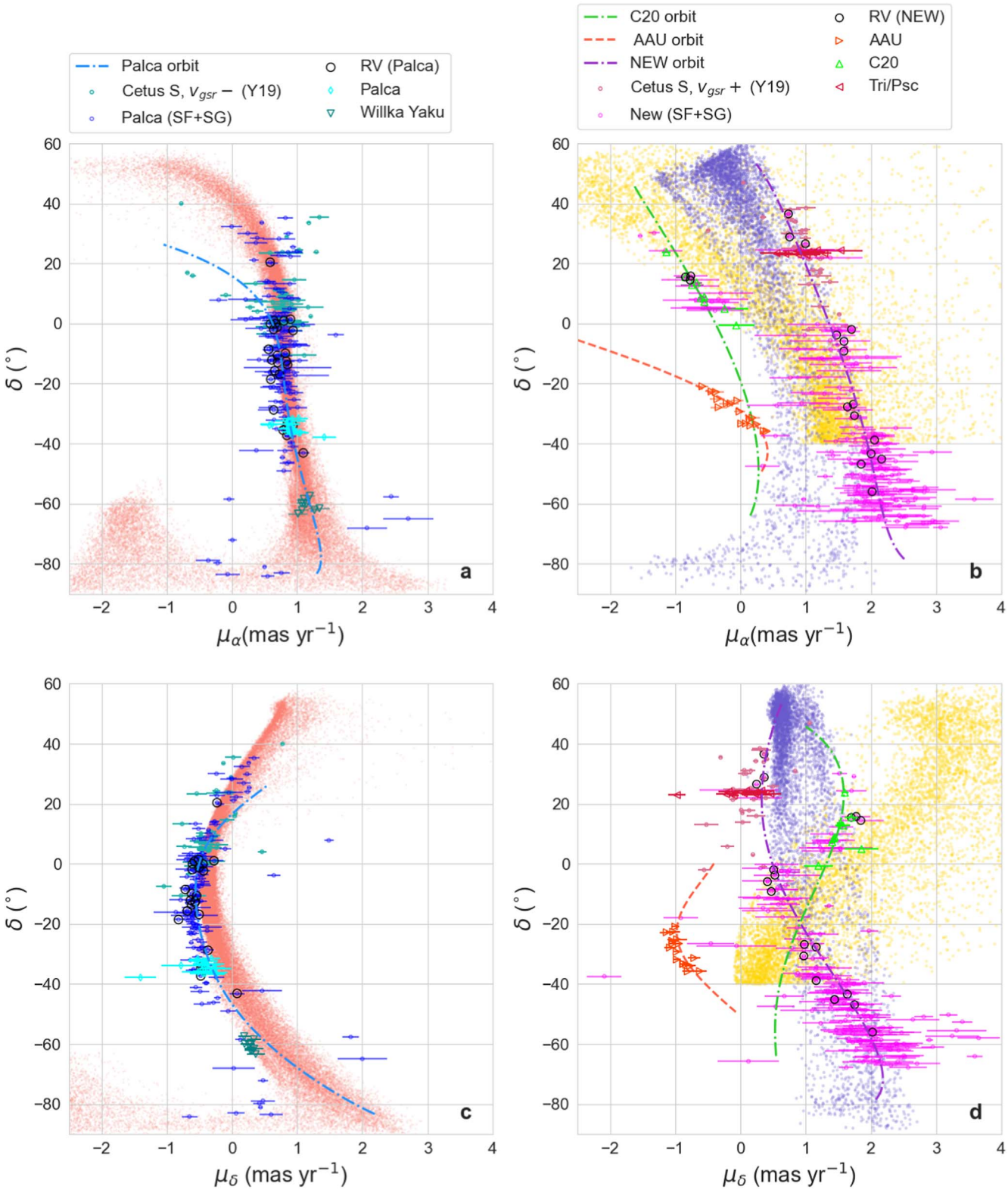

Figure 7. Same as Figure 6 in proper motion spaces, (δ, μ_α) and (δ, μ_δ). (a) and (c) Cetus from Y19 (negative $v_{\rm gsr}$, green), the Palca wrap detected in this work (blue), and the Palca (cyan diamonds) and Willka Yaku (dark green inverted triangles) streams from S5 (Li et al. 2021) form a continuous stream track, and agree with the averaged sampling orbit of the Palca wrap as well as T1 (orange). (b) and (d) Cetus (positive $v_{\rm gsr}$, pink), the new southern wrap (magenta), and its orbit (purple), and the Tri/Psc stream (red left triangles) align with T2 (light purple). C-20 (light green) and its best-fitting orbit (green) generally agree with L1 (yellow), whereas AAU and its fitted orbit (orange) deviate further from L1.

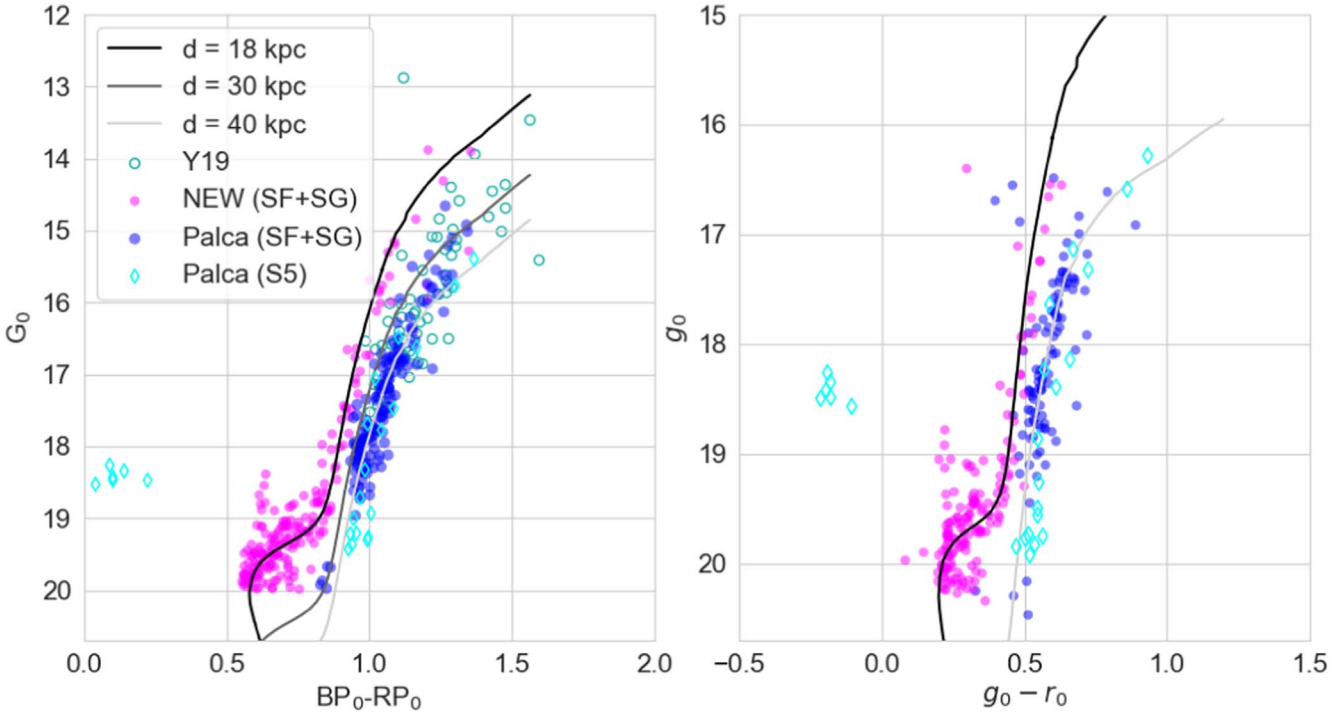

Figure 8. CMD of the Cetus members from Gaia EDR3 (left panel) and DES DR2 (right panel), where the magnitudes and colors are extinction-corrected values. The Palca wrap (blue solid circles) matches the PARSEC isochrone (age = 12.5 Gyr, [Fe/H] = −2) at $d = 40$ kpc, which is the average heliocentric distance of the Palca members estimated. The new southern wrap (magenta solid circles) is consistent with the same isochrone at $d = 18$ kpc. The previous Cetus K Giant members (open green circles) follows the isochrone at $d = 30$ kpc.

The Cetus-New wrap also stretches over 100° in the same part of the sky as the Cetus-Palca wrap. The whole wrap aligns with the averaged sampling orbit (purple dashed–dotted line) of the new southern wrap, and also agrees with the second wrap in the trailing arm (T2; light purple). The Tri/Psc stream is located in the footprint of Cetus in the northern sky and has very similar proper motion measurements to the northern Cetus with positive $v_{\rm gsr}$.

The C-20 stream and its best-fit orbit (turquoise line) follow similar tracks to the first wrap in the leading arm (L1; yellow). Although the AAU stream and its best-fit orbit (orange line) follows L1 closely in (b, d, $v_{\rm gsr}$) space, they show different tracks in the proper motion space. We reach the conclusion that we cannot rule out the possibility that the AAU stream is associated with the Cetus system, but this association is weaker compared to that of C-20 with the Cetus stream.

6. Mass of the Cetus Progenitor

We have shown that the southern part of the Cetus stream detected in this work has two wraps located at different distances. This can also be seen from their color–magnitude diagrams (CMD) in Figure 8, where we plot the southern Cetus members using Gaia EDR3 (Riello et al. 2021) and DES DR2 photometry (Abbott et al. 2021). After correcting for the extinction (see details in Section 3.2), the Palca (blue) and the new southern wrap (magenta) are consistent with the PARSEC isochrones ([Fe/H] = −2, age = 12.5 Gyr) assuming the initial mass function from Kroupa (2001, 2002) at $d = 40$ kpc (black) and $d = 18$ kpc (light gray), respectively. These distances are the averages of all members in each of these two wraps estimated from Gaia EDR3 photometry (see details in Section 3.2). The Palca members from Li et al. (2021) are represented by open cyan diamonds and are consistent with the isochrone at $d = 40$ kpc. The previous Cetus members from Y19 (open green circles) are in agreement with the isochrone (medium gray) at their average distance of $d = 30$ kpc.

To estimate the minimum total luminosity of the Cetus progenitor, we sum the fluxes of all stars brighter than $G_0 = 20$ in the Palca wrap, and those brighter than $G_0 = 18.5$ in the new southern wrap. For the K giant members from Y19, we sum the flux of those brighter than $G_0 = 17$ mag. We then obtain the correction factor by summing, for each sample, the fluxes of stars fainter than these magnitudes according to the luminosity function of the stellar population that corresponds to the isochrone shown in Figure 8. The total corrected luminosity of these two wraps combined with the previous K giant members is $10^{5.4} L_{\odot}$. This gives us a lower mass limit for the Cetus progenitor, $M_V = -8.7$, and $M_* = 10^{5.6}\, M_{\odot}$, assuming a stellar mass-to-light ratio of 1.6 for dwarf galaxies as given in Woo et al. (2008). We then compare this value with the luminosity–metallicity relation of the Milky Way satellite dwarf galaxies in Figure 9 (see, e.g., Battaglia et al. 2021, and references within), where the lower limit on the total magnitude of the Cetus progenitor is denoted by the magenta circle and a right arrow. This lower limit is compatible with the distribution of Milky Way dwarf galaxies in this plane and could imply that the progenitor of Cetus was not significantly more massive than a dwarf spheroidal galaxy (dSph) like Draco or Ursa Minor ($\sim 10^{5.7} M_{\odot}$ Kirby et al. 2013).

7. Discussions and Conclusions

In this study, we made a fusion of `StreamFinder` and `StarGO` to search for members of the Cetus system in the all-sky Gaia EDR3 data. We confirm that the Palca stream discovered by Shipp et al. (2018) and further studied by Chang

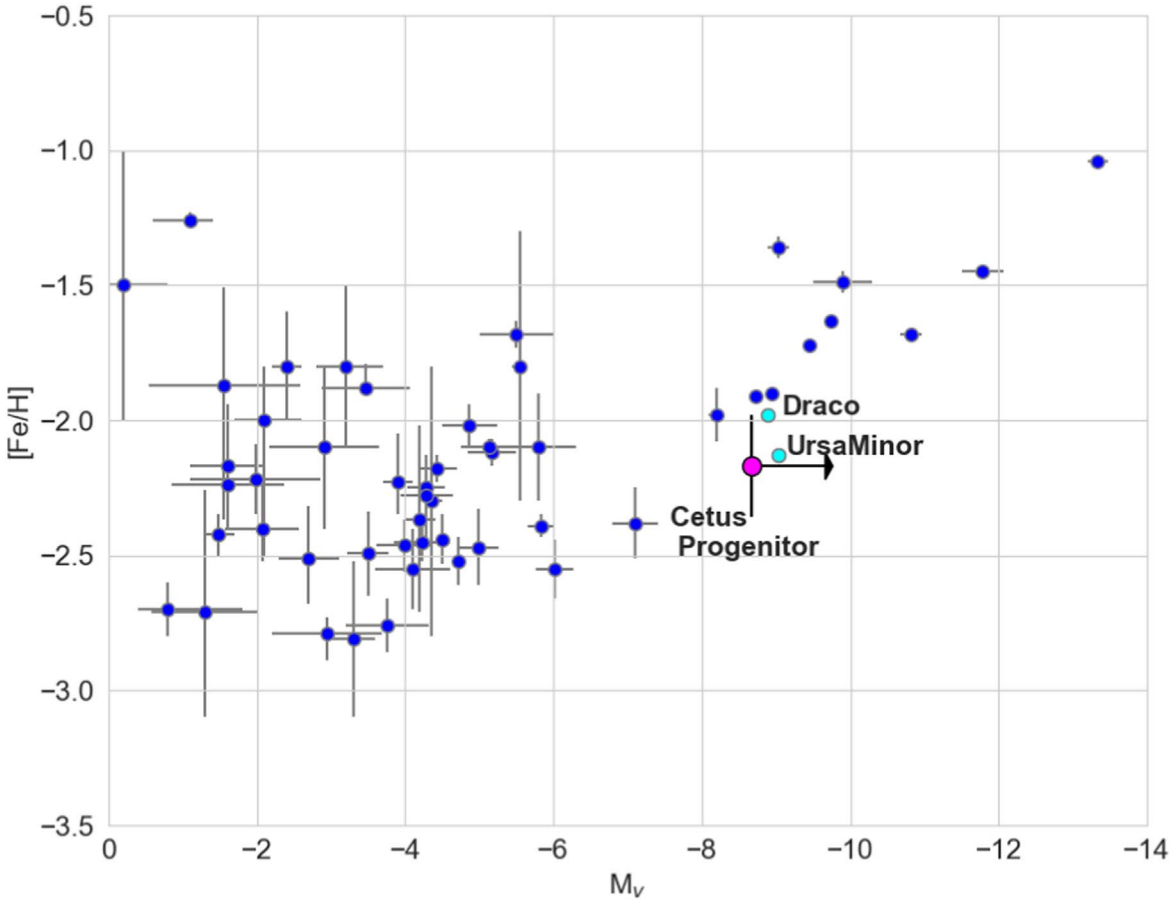

Figure 9. Luminosity–metallicity plot of classical dSphs and ultra-faint dwarfs (see Battaglia et al. 2021, and references within). The lower mass limit of the Cetus progenitor is shown as a magenta circle with a right arrow, which lies in the low-mass classical dSph regime, close to the Ursa Minor and Draco dSphs.

et al. (2020) and Li et al. (2021) is the southern extension of the Cetus component with negative $v_{\rm gsr}$ detected by Y19. We identify 160 candidate members that belong to the Cetus-Palca stream wrap in the distance range of 30–60 kpc and in the sky coverage of $-40^\circ < \delta < 40^\circ$. The Willka Yaku stream is shown to be confidently associated with the Cetus-Palca wrap, and extends the structure 20° in the southern sky. We also present accurate line-of-sight velocities for 26 stars in this wrap from different spectroscopic surveys and follow-up observations, and show that their orbits are consistent with the first wrap in the trailing arm of the Cetus model of Chang et al. (2020).

Furthermore, we identify a second, densely populated southern wrap with 205 stars, overlapping the Palca wrap on the sky, but located much closer, at an average distance of 18 kpc. Based on 18 stars with line-of-sight velocities, we show that these are the extension of the previously detected Cetus stream with positive $v_{\rm gsr}$, and have a strong association with the Tri/Psc stream. The Cetus-New wrap spreads over 100° on the sky, and matches perfectly the second wrap in the trailing arm of the Cetus model.

Our exploration also highlights a thin stream that belongs to the same system in the northern sky. It coincides with the thin stream C-20 discovered by STREAMFINDER in Ibata et al. (2021). We confirm that C-20 is dynamically associated with the Cetus system from its nine members with line-of-sight velocity information. Thus, it is the second most confidently associated structure after globular cluster NGC 5824. The best-fit orbit of C-20 shows that it was possibly stripped with the first wrap in the leading arm.

The association between the Cetus system and the ATLAS-Aliqa-Uma stream is weaker compared to the other associations described above. However, the best-fit orbit still closely follows the first leading wrap. The observed *kink* features and gaps of the AAU stream suggest that it might have been perturbed, potentially by a small mass dark matter halo. Li et al. (2021) suggested that it could be due to an encounter with the Sagittarius dwarf galaxy. Given the proximity of the orbits of the AAU and the Cetus system, we propose a scenario where the perturber is the shredded dark matter halo of the Cetus progenitor. We will investigate this possible connection in future studies.

Based on the members of the southern Cetus stream from Y19 and this study, we measure its average metallicity, $[{\rm Fe/H}] = -2.17 \pm 0.2$ and we estimate a lower limit to its total luminosity ($M_V = -8.7$). As such, the Cetus progenitor is compatible with other Milky Way satellite galaxies similar to the Ursa Minor dwarf galaxy with stellar mass $\sim 10^{5.7}\,M_\odot$. In this case, NGC 5824, as the most confident associate, has a similar stellar mass ($10^6\,M_\odot$) to the Cetus progenitor. How such a massive globular cluster is associated with the progenitor system remains puzzle if our estimates are accurate.

The scenario of NGC 5824 being the nuclear star cluster of the Cetus progenitor is disfavored by the *N*-body modeling of the Cetus stream detected in the northern sky (Chang et al. 2020). A key conclusion of this work is that the center of the

disrupted progenitor cannot be at the location of NGC 5824 in order to populate streams in the detected region instead of the region around NGC 5824. In this work, we identify the two southern wraps as the extent of the Cetus stream that are predicted by the favored model from Chang et al. (2020). At the same time, we still do not detect any densely populated structure around NGC 5824, even though the cluster falls within the coverage of the data we used. All of these lines of evidences support the scenario that NGC 5824 is not the core of the Cetus progenitor. On the other hand, the progenitor would need to have been more massive than $10^6\,M_\odot$ in stellar mass to host NGC 5824 as its nuclear star cluster. According to the nuclei to stellar mass relation given by Georgiev et al. (2016), a nuclear star cluster of $\sim 10^6\,M_\odot$ is typically hosted by a galaxy of at least $10^8\,M_\odot$ and thus much more massive than our estimate of the Cetus progenitor. We therefore conclude that it is unlikely that NGC 5824 was the former nucleus or a globular cluster of the Cetus progenitor. However, due to its very similar dynamical properties we think it is probable that it was accreted with the group of satellites that included the Cetus progenitor.

Finally, we also identify another three associated substructures (Tri/Psc, Willka Yaku, C-20) that, given their morphology, are very likely globular cluster streams. They belong to the stream wraps of the Cetus system that are closer to the predicted center compared to NGC 5824 according to the Cetus model. Contrary to what we discussed above for NGC 5824, it appears natural to associate these apparently smaller systems to the progenitor of Cetus. It is likely that their progenitors were less massive than $10^5\,M_\odot$ because such globular clusters typically dissolve within a Hubble time due to internal dynamical effects (see, e.g., Baumgardt & Makino 2003; Kruijssen 2019). Based on the stellar mass and the *N*-body model, we estimate a total dark matter halo mass of the Cetus progenitor is around $10^9\,M_\odot$ (see, e.g., Read et al. 2017). It is known from observations of galaxies in the Local Universe that the stellar mass of the whole globular cluster system of a galaxy is a factor of 10^{-4} smaller than the total halo mass of its galaxy (Harris et al. 2013). This scenario, in which the progenitor globular clusters have a combined mass of $\sim 10^5\,M_\odot$, is, while speculative, consistent with having been members of the Cetus progenitor.

The Cetus system is a perfect example of a dwarf galaxy that has undergone several orbital periods of stripping and that left behind complex stellar debris in the form of multiple wraps around the Galaxy. It further confirms the complexity of mapping the various structures of the Milky Way stellar halo and how streams that appear separated in the sky, identified from various data sets with different techniques, can actually be produced by the same accretion event. Revealing this common origin strongly benefits from exploring the dynamical properties of their component stars, as we did here by combining `STREAMFINDER` and `StarGO`. The *N*-body simulation tailored to the originally discovered parts of the stream is also a very powerful tool that provides insight into how the different pieces of the debris fit together. Only through such multi-approach studies can we hope to understand how progenitors were shredded during their long disruptive history.

Z.Y. wishes to thank Guillaume F. Thomas for helpful comments when drafting the paper. Z.Y., R.A.I., N.F.M., A.A., and B.F. acknowledge the European Research Council (ERC) under the European Unions Horizon 2020 research and innovation program (grant agreement No. 834148). Z.Y., R.A..I, N.F.M., E.C., and P.B. also acknowledge funding from the Agence Nationale de la Recherche (ANR project ANR-18-CE31-0017). K.M. acknowledges support from the Alexander von Humboldt Foundation at Max-Planck-Institut für Astronomie, Heidelberg. K.M. is also grateful to the IAU's Gruber Foundation Fellowship Program for financial support. E.C. and P.B. to the list of people supported by ANR-18-CE31-0017. M.B. acknowledges the support to this research by the PRIN INAF 2019 grant ObFu 1.05.01.85.14 ("Building up the halo: chemo-dynamical tagging in the age of large surveys," PI. S. Lucatello). Y.H. is supported by National Key R&D Program of China No. 2019YFA0405500 and National Natural Science Foundation of China grant Nos. 11903027, 11833006, and 11973001. E.S. acknowledges funding through VIDI grant "Pushing Galactic Archaeology to its limits" (with project No. VI.Vidi.193.093), which is funded by the Dutch Research Council (NWO). D.A. acknowledges support from the ERC Starting Grant NEFERTITI H2020/808240.

We gratefully acknowledge the High Performance Computing center of the Université de Strasbourg for a very generous time allocation and for their support over the development of this project.

This work has made use of data from the European Space Agency (ESA) mission Gaia (https://www.cosmos.esa.int/gaia), processed by the Gaia Data Processing and Analysis Consortium (DPAC, https://www.cosmos.esa.int/web/gaia/dpac/consortium). Funding for the DPAC has been provided by national institutions, in particular the institutions participating in the Gaia Multilateral Agreement.

Based on observations collected at the European Southern Observatory under ESO programs 0105.B-0235(A) and 0108.B-0431(A).

Based on data acquired at the Anglo-Australian Telescope. We acknowledge the traditional owners of the land on which the AAT stands, the Gamilaraay people, and pay our respects to elders past and present.

Software: STREAMFINDER (Malhan & Ibata 2018), StarGO (Yuan et al. 2018), AGAMA (Vasiliev 2019), astropy (Astropy Collaboration 2018), galpy (Bovy 2015), IRAF (Tody 1986, 1993), NumPy van der Walt et al. (2011), SciPy (Jones et al. 2001), matplotlib (Hunter 2007), and seaborn (Waskom et al. 2016).

Data Availability

We publish the Cetus model from Chang et al. (2020) used in this study. The catalog of 2×10^5 star particles in the last snapshot of *N*-body simulation is hosted at 10.5281/zenodo.5771585.

ORCID iDs

Zhen Yuan https://orcid.org/0000-0002-8129-5415
Khyati Malhan https://orcid.org/0000-0002-8318-433X
Rodrigo A. Ibata https://orcid.org/0000-0002-3292-9709
Nicolas F. Martin https://orcid.org/0000-0002-1349-202X
Piercarlo Bonifacio https://orcid.org/0000-0002-1014-0635
Michele Bellazzini https://orcid.org/0000-0001-8200-810X
Karina Voggel https://orcid.org/0000-0001-6215-0950
Amandine Doliva-Dolinsky https://orcid.org/0000-0001-9775-9029
Julio Navarro https://orcid.org/0000-0003-3862-5076
Benoit Famaey https://orcid.org/0000-0003-3180-9825
David S. Aguado https://orcid.org/0000-0001-5200-3973

References

Abbott, T. M. C., Adamów, M., Aguena, M., et al. 2021, ApJS, 255, 20
Aguado, D. S., Belokurov, V., Myeong, G. C., et al. 2021a, ApJL, 908, L8
Aguado, D. S., Myeong, G. C., Belokurov, V., et al. 2021b, MNRAS, 500, 889
Amorisco, N. C. 2017, MNRAS, 464, 2882
Astropy Collaboration 2018, AJ, 156, 123
Battaglia, G., Taibi, S., Thomas, G. F., & Fritz, T. K. 2022, A&A, 657, A54
Baumgardt, H., & Makino, J. 2003, MNRAS, 340, 227
Bechtol, K., Drlica-Wagner, A., Balbinot, E., et al. 2015, ApJ, 807, 50
Beers, T. C., & Christlieb, N. 2005, ARA&A, 43, 531
Bekki, K., & Freeman, K. C. 2003, MNRAS, 346, L11
Bellazzini, M., Ibata, R., Malhan, K., et al. 2020, A&A, 636, A107
Belokurov, V., Erkal, D., Evans, N. W., Koposov, S. E., & Deason, A. J. 2018, MNRAS, 478, 611
Belokurov, V., Zucker, D. B., Evans, N. W., et al. 2006, ApJL, 647, L111
Bonaca, A., Conroy, C., Price-Whelan, A. M., & Hogg, D. W. 2019, ApJL, 881, L37
Bonaca, A., Geha, M., & Kallivayalil, N. 2012, ApJL, 760, L6
Bonaca, A., Naidu, R. P., Conroy, C., et al. 2021, ApJL, 909, L26
Bovill, M. S., & Ricotti, M. 2009, ApJ, 693, 1859
Bovy, J. 2015, ApJS, 216, 29
Bressan, A., Marigo, P., Girardi, L., et al. 2012, MNRAS, 427, 127
Brown, T. M., Tumlinson, J., Geha, M., et al. 2014, ApJ, 796, 91
Buder, S., Lind, K., Ness, M. K., & Feuillet, D. K. 2022, MNRAS, 510, 2407
Bullock, J. S., & Boylan-Kolchin, M. 2017, ARA&A, 55, 343
Bullock, J. S., & Johnston, K. V. 2005, ApJ, 635, 931
Chambers, K. C., Magnier, E. A., Metcalfe, N., et al. 2016, arXiv:1612.05560
Cui, X.-Q., Zhao, Y.-H., Chu, Y.-Q., et al. 2012, RAA, 12, 1197
Chang, J., Yuan, Z., Xue, X.-X., et al. 2020, ApJ, 905, 100
The Dark Energy Survey Collaboration 2005, arXiv:astro-ph/0510346
Deason, A. J., Belokurov, V., & Evans, N. W. 2011, MNRAS, 416, 2903
The DES Collaboration, Drlica-Wagner, A., Bechtol, K., et al. 2015, ApJ, 813, 109
Dierickx, M. I. P., & Loeb, A. 2017, ApJ, 836, 92
Donlon, T., II, Newberg, H. J., Sanderson, R., & Widrow, L. M. 2020, ApJ, 902, 119
Duch, W., & Naud, A. 1996, Proc. Second Conf. on Neural Networks and Their Applications *(Orle Gniazdo, Poland)* 138
Gaia Collaboration, Brown, A. G. A., Vallenari, A., & Prusti, T. 2018, A&A, 616, A1
Gaia Collaboration, Prusti, T., de Bruijne, J. H. J., Brown, A. G. A., & Vallenari, A. 2016, A&A, 595, A1
Georgiev, I. Y., Böker, T., Leigh, N., Lützgendorf, N., & Neumayer, N. 2016, MNRAS, 457, 2122
Gudin, D., Shank, D., Beers, T. C., et al. 2021, ApJ, 908, 79
Gull, M., Frebel, A., Hinojosa, K., et al. 2021, ApJ, 912, 52
Harris, W. E., Harris, G. L. H., & Alessi, M. 2013, ApJ, 772, 82
Helmi, A., Babusiaux, C., Koppelman, H. H., et al. 2018, Natur, 563, 85
Helmi, A., White, S. D. M., de Zeeuw, P. T., & Zhao, H. 1999, Natur, 402, 53
Huang, Y., Beers, T. C., Wolf, C., et al. 2022, ApJ, 925, 164
Huang, Y., Yuan, H., Li, C., et al. 2021, ApJ, 907, 68
Hunter, J. D. 2007, CSE, 9, 90
Ibata, R., Irwin, M., Lewis, G. F., & Stolte, A. 2001, ApJL, 547, L133
Ibata, R., Malhan, K., Martin, N., et al. 2021, ApJ, 914, 123
Ibata, R. A., Bellazzini, M., Malhan, K., Martin, N., & Bianchini, P. 2019a, NatAs, 3, 667
Ibata, R. A., Malhan, K., & Martin, N. F. 2019b, ApJ, 872, 152
Ibata, R. A., Malhan, K., Martin, N. F., & Starkenburg, E. 2018, ApJ, 865, 85
Ideta, M., & Makino, J. 2004, ApJL, 616, L107
Irwin, M. J., Belokurov, V., Evans, N. W., et al. 2007, ApJL, 656, L13
Ji, A. P., Li, T. S., Hansen, T. T., et al. 2020, AJ, 160, 181
Johnston, K. V. 1998, ApJ, 495, 297
Jones, E., Oliphant, T., Peterson, P., et al. 2001, SciPy: Open Source Scientific Tools for Python, http://www.scipy.org/
Kirby, E. N., Cohen, J. G., Guhathakurta, P., et al. 2013, ApJ, 779, 102
Kohonen, T. 1982, Biological Cybernetics, 43, 59
Koposov, S., Belokurov, V., Evans, N. W., et al. 2008, ApJ, 686, 279
Koposov, S. E., Belokurov, V., Torrealba, G., & Evans, N. W. 2015, ApJ, 805, 130
Koppelman, H. H., Helmi, A., Massari, D., Price-Whelan, A. M., & Starkenburg, T. K. 2019, A&A, 631, L9
Kroupa, P. 2001, MNRAS, 322, 231
Kroupa, P. 2002, Sci, 295, 82
Kruijssen, J. M. D. 2019, MNRAS, 486, L20
Laevens, B. P. M., Martin, N. F., Bernard, E. J., et al. 2015, ApJ, 813, 44
Law, D. R., & Majewski, S. R. 2010, ApJ, 714, 229
Li, H., Tan, K., & Zhao, G. 2018, ApJS, 238, 16
Li, T. S., Balbinot, E., Mondrik, N., et al. 2016, ApJ, 817, 135
Li, T. S., Ji, A. P., Pace, A. B., et al. 2022, ApJ, 928, 30
Li, T. S., Koposov, S. E., Erkal, D., et al. 2021, ApJ, 911, 149
Li, T. S., Koposov, S. E., Zucker, D. B., et al. 2019, MNRAS, 490, 3508
Limberg, G., Rossi, S., Beers, T. C., et al. 2021, ApJ, 907, 10
Majewski, S. R., Skrutskie, M. F., Weinberg, M. D., & Ostheimer, J. C. 2003, ApJ, 599, 1082
Malhan, K., & Ibata, R. A. 2018, MNRAS, 477, 4063
Malhan, K., Ibata, R. A., & Martin, N. F. 2018, MNRAS, 481, 3442
Malhan, K., Yuan, Z., Ibata, R. A., et al. 2021, ApJ, 920, 51
Martin, C., Carlin, J. L., Newberg, H. J., & Grillmair, C. 2013, ApJL, 765, L39
Martin, N. F., Collins, M. L. M., Longeard, N., & Tollerud, E. 2018, ApJL, 859, L5
Martin, N. F., Ibata, R. A., Rich, R. M., & Collins, M. L. M. 2014, ApJ, 787, 19
Martin, N. F., Ibata, R. A., Starkenburg, E., et al. 2022a, arXiv:2201.01310
Martin, N. F., Nidever, D. L., Besla, G., & Olsen, K. 2015, ApJL, 804, L5
Martin, N. F., Venn, K. A., Aguado, D. S., et al. 2022b, Natur, 601, 45
Massari, D., Koppelman, H. H., & Helmi, A. 2019, A&A, 630, L4
Mateo, M., Mirabal, N., Udalski, A., et al. 1996, ApJL, 458, L13
Matsuno, T., Aoki, W., & Suda, T. 2019, ApJL, 874, L35
Matsuno, T., Hirai, Y., Tarumi, Y., et al. 2021, A&A, 650, A110
McMillan, P. J. 2017, MNRAS, 465, 76
Mizutani, A., Chiba, M., & Sakamoto, T. 2003, ApJL, 589, L89
Monachesi, A., Gómez, F. A., Grand, R. J. J., et al. 2019, MNRAS, 485, 2589
Mucciarelli, A., Lapenna, E., Ferraro, F. R., & Lanzoni, B. 2018, ApJ, 859, 75
Myeong, G. C., Evans, N. W., Belokurov, V., Amorisco, N. C., & Koposov, S. E. 2018a, MNRAS, 475, 1537
Myeong, G. C., Evans, N. W., Belokurov, V., Sanders, J. L., & Koposov, S. E. 2018b, ApJL, 863, L28
Myeong, G. C., Vasiliev, E., Iorio, G., Evans, N. W., & Belokurov, V. 2019, MNRAS, 488, 1235
Naidu, R. P., Conroy, C., Bonaca, A., & Johnson, B. D. 2020, ApJ, 901, 48
Newberg, H. J., Yanny, B., & Willett, B. A. 2009, ApJL, 700, L61
Peñarrubia, J., Belokurov, V., Evans, N. W., et al. 2010, MNRAS, 408, L26
Price-Whelan, A. M., & Bonaca, A. 2018, ApJL, 863, L20
Read, J. I., Iorio, G., Agertz, O., & Fraternali, F. 2017, MNRAS, 467, 2019
Riello, M., De Angeli, F., & Evans, D. W. 2021, A&A, 649, A3
Roederer, I. U., Hattori, K., & Valluri, M. 2018, AJ, 156, 179
Roederer, I. U., Mateo, M., Bailey, J. I. I., et al. 2016, AJ, 151, 82
Sbordone, L., Caffau, E., Bonifacio, P., & Duffau, S. 2014, A&A, 564, A109
Schlafly, E. F., & Finkbeiner, D. P. 2011, ApJ, 737, 103
Schlegel, D. J., Finkbeiner, D. P., & Davis, M. 1998, ApJ, 500, 525
Sestito, F., Longeard, N., Martin, N. F., et al. 2019, MNRAS, 484, 2166
Sestito, F., Martin, N. F., Starkenburg, E., & Arentsen, A. 2020, MNRAS, 497, L7
Shank, D., Beers, T. C., Placco, V. M., et al. 2022, ApJ, 926, 26
Shipp, N., Drlica-Wagner, A., Balbinot, E., & Ferguson, P. 2018, ApJ, 862, 114
Simon, J. D. 2019, ARA&A, 57, 375
Simpson, J. D., Martell, S. L., Buder, S., et al. 2021, MNRAS, 507, 43
Starkenburg, E., Martin, N., Youakim, K., et al. 2017, MNRAS, 471, 2587
Tody, D. 1986, Proc. SPIE, 627, 733
Tody, D. 1993, in ASP Conf. Ser. 52, Astronomical Data Analysis Software and Systems II, ed. R. J. Hanisch, R. J. V. Brissenden, & J. Barnes (San Francisco, CA: ASP), 173
Tsuchiya, T., Korchagin, V. I., & Dinescu, D. I. 2004, MNRAS, 350, 1141
van der Walt, S., Colbert, S. C., & Varoquaux, G. 2011, CSE, 13, 22
Vasiliev, E. 2019, MNRAS, 482, 1525
Vasiliev, E., & Baumgardt, H. 2021, MNRAS, 505, 5978
Vasiliev, E., Belokurov, V., & Erkal, D. 2021, MNRAS, 501, 2279
Vera-Ciro, C., & Helmi, A. 2013, ApJL, 773, L4
Wan, Z., Lewis, G. F., Li, T. S., et al. 2020, Natur, 583, 768
Waskom, M., Botvinnik, O., drewokane, et al. 2016, Seaborn, v0.7.0, Zenodo, doi:10.5281/zenodo.45133
Willman, B., Blanton, M. R., West, A. A., et al. 2005a, AJ, 129, 2692
Willman, B., Dalcanton, J. J., Martinez-Delgado, D., et al. 2005b, ApJL, 626, L85
Woo, J., Courteau, S., & Dekel, A. 2008, MNRAS, 390, 1453
Yanny, B., Rockosi, C., Newberg, H. J., et al. 2009, AJ, 137, 4377
York, D. G., Adelman, J., Anderson, J. E., Jr., et al. 2000, AJ, 120, 1579
Yuan, Z., Chang, J., Banerjee, P., et al. 2018, ApJ, 863, 26
Yuan, Z., Chang, J., Beers, T. C., & Huang, Y. 2020a, ApJL, 898, L37
Yuan, Z., Myeong, G. C., Beers, T. C., et al. 2020b, ApJ, 891, 39
Yuan, Z., Smith, M. C., Xue, X.-X., et al. 2019, ApJ, 881, 164
Zhao, G., Zhao, Y.-H., Chu, Y.-Q., Jing, Y.-P., & Deng, L.-C. 2012, RAA, 12, 723